# Potential sources of predictive skill of seasonal precipitation forecasts for Suriname

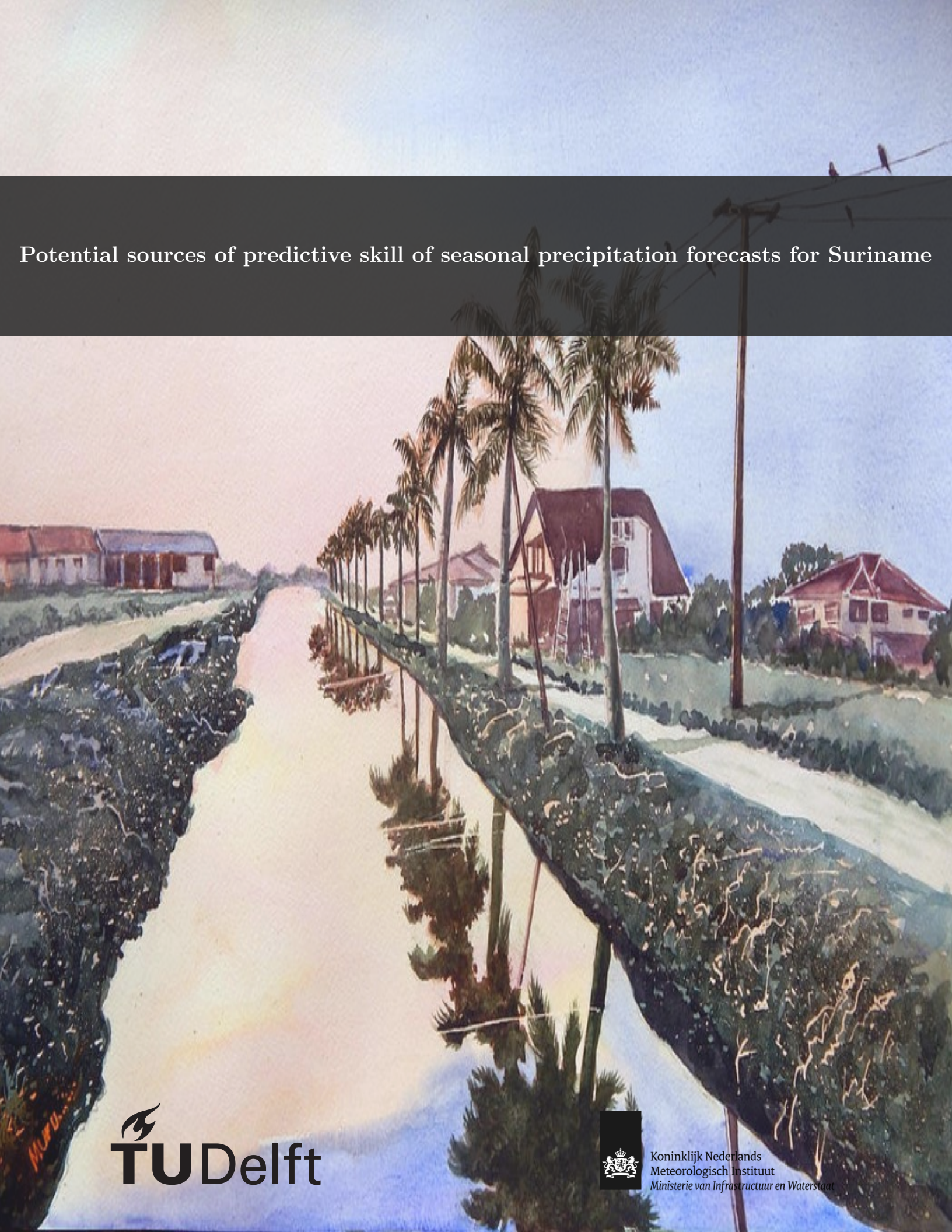

TU Delft

Koninklijk Nederlands
Meteorologisch Instituut
*Ministerie van Infrastructuur en Waterstaat*

# Potential sources of predictive skill of seasonal precipitation forecasts for Suriname

A study on the dynamics of seasonal precipitation in Suriname with the help of moisture tracking and Sea Surface Temperature correlations.

by

E.C. Koole

to obtain the degree of Master of Science
at the Delft University of Technology,
to be defended publicly on Wednesday August 30, 2023 at 10:30 AM.


| | | |
|---|---|---|
| Student number: | 4381939 | |
| Project duration: | January, 2023 – August, 2023 | |
| Thesis committee: | Dr. ir. M.M. Rutten, | TU Delft, chair |
| | Dr. R. Haarsma, | KNMI |
| | Dr. ir. R. van der Ent, | TU Delft |


An electronic version of this thesis is available at http://repository.tudelft.nl/.



Cover image: 'Evening Light Paramaribo Suriname' - Murugesan A., 2014

# Acknowledgements

Hereby, I present to you my master thesis. This master thesis is a part of the finalization of the Environmental Engineering track of the Civil Engineering master. With this final work of art my time as a student has come to an end. A time at Delft University of Technology that I enjoyed, especially when finding out which topics excite me. Climate change, hydrology and extreme weather events are definitely on that list.

Working on my master thesis has been challenging and full of learning opportunities. As well in exploring new grounds of meteorology and ocean dynamics as in personal development. I am grateful for the opportunity to have been able to work and learn at the Koninklijk Nederlands Meteorologisch Instituut (KNMI) and to have Rein Haarsma as my supervisor there. Everybody I met at the KNMI shows enthusiasm for their expertise, which is a very pleasant surrounding to be working in. Thank you Rein for the discussions about meteorology and oceanography. Topics that were quit new to me, but you helped me navigate them.

A special thank you also to Martine Rutten. Your enthusiasm, critical feedback and care were highly appreciated. I am thankful for the opportunity you created to connect my work to other people working on similar topics in Suriname and the Anton de Kom University in Paramaribo. To Ruud van der Ent I am grateful for the introduction into the WAM2layers moisture tracking model and the feedback you provided to my work.

Finally, I would like to thank my family and friends for their support. I could both share my enthusiasm about the topic as well as my frustrations when it didn't go as planned and you were always there to listen.

# Abstract

This study investigates the dynamics of seasonal precipitation in Suriname with the help of moisture tracking and Sea Surface Temperature correlations. Prolonged drought periods, heavy precipitation events and accompanying flash floods and landslides are expected to increase in Suriname in the coming years. Reliable seasonal precipitation forecasts are therefore of great value to the agriculture, livestock and energy sectors in Suriname, but also for drought and flood mitigation. The objective of this study is to look into the sources of the predictive skill for seasonal precipitation forecasts for Suriname.

First, Spearman rank correlation analysis between sea surface temperature anomalies and Suriname precipitation anomalies was performed to establish the potential for statistical seasonal precipitation forecasts from SSTs. Second, moisture tracking with the model WAM2layers was applied to find the origin areas of evaporation for precipitation in Suriname. At last, these patterns of correlation and moisture tracking were combined with composite data to determine which potential drivers are influencing the precipitation anomalies in Suriname.

The results show that the ASON season displays the largest SST correlations (0.4 for NiÑo3 and Niño3.4 index with a lag of 3 months) and the longest lag time at which correlations are visible. This is due to the significant influence of ENSO on the ASON season precipitation. The DJFM season shows a clear link towards the Tropical Atlantic Variability and especially the AMM mode. Positive (negative) SST in the tropical north Atlantic cause a northward (southward) shift of the ITCZ over Suriname. The AMJJ season reveals the smallest skill to predict seasonal precipitation anomalies. This could possibly be enhanced by performing a sub-seasonal analysis.

The processes of potential skill found in this thesis report can be of help to forecasters for the improvement of seasonal precipitation forecasts for Suriname.

# Contents

# List of abbreviations

| Acronym | Definition |
|---|---|
| **ABF** | Angola-Benguela Front |
| **ACT** | Atlantic Cold Tongue |
| **AMM** | Atlantic Meridional Mode |
| **AZM** | Atlantic Zonal Mode |
| **CDO** | Climate Data Operators |
| **CHIRPS** | Climate Hazards Group InfraRed Precipitation with Station data |
| **CRU** | Climatic Research Unit TS v.4.06 |
| **ENSO** | El Niño Southern Oscillation |
| **ERA5** | ECMWF Re-Analysis v5 |
| **GHCNm** | Global Historical Climatology Network monthly version |
| **GPCC** | Global Precipitation Climatology Centre version 2022 |
| **GPCP** | Global Precipitation Climatology Project |
| **GridPrecip** | Gridded Precipitation datasets |
| **ITCZ** | Intertropical Convergence Zone |
| **KNMI** | Koninklijk Nederlands Meteorologisch Instituut |
| **LACA&D** | Latin America Climate Assessment & Dataset |
| **MDS** | Meteorologische Dienst Suriname |
| **NAO** | North Atlantic Oscillation |
| **SACZ** | South Atlantic Convergence Zone |
| **SAMS** | South American Monsoon System |
| **SLP** | Sea Level Pressure |
| **SST** | Sea Surface Temperature |
| **SSTA** | Sea Surface Temperature Anomaly |
| **TAMG** | Tropical Atlantic Meridional Gradient |
| **TAV** | Tropical Atlantic variability |
| **TNA** | Tropical North Atlantic |
| **TSA** | Tropical South Atlantic |

# 1 Introduction

Precipitation is the main resource for both surface- and groundwater in Suriname. This results in a great dependency for many sectors on the amount and timing of precipitation. Changes in the precipitation characteristics are of great influence to the agriculture, livestock and energy sectors, but also for the design and operation of hydraulic structures in the river basins and coastal areas as drought and flood mitigation (Ferreira et al., 2022; Naipal & Nurmohamed, 2004). Individual weather patterns are known to lack predictability beyond a period of approximately two weeks due to their nonlinear behaviour (Lorenz, 1982). On the other hand, the seasonal climate in tropical regions exhibits predictability over extended time frames due to the impact of boundary forcing mechanisms such as sea surface temperature. To have reliable seasonal precipitation forecasts (referring to the forthcoming 2-4 months) would equip various sectors with more knowledge on the timing and management of their operations.

The main goal of seasonal precipitation forecasts is to provide the projected anomalies to the climatology's mean precipitation values. Seasonal forecasts are currently either performed by General Circulation Models (GCM's) or statistical models based on correlations between predictands, the variable to be predicted, and predictors, the variable used to make the forecast. Statistical downscaling of dynamically forecast variables such as SST can also be applied. At the moment there are multiple international providers of seasonal forecast models. The most advanced and evaluated are the North American Multi-Model Ensemble (NMME) and the Copernicus Climate Change Service (C3S) multi-system seasonal forecast. Seasonal precipitation forecasts for Suriname are produced by the Caribbean Institute for Meteorology and Hydrology (CIMH). The CIMH has been producing downscaled probabilistic tercile precipitation outlooks for the Caribbean since 2000. Tercile forecast predictions are made for below normal, normal and above normal precipitation. The seasonal outlooks are made with a statistical model using Canonical Correlation Analysis (CCA) run with the International Research Institute for Climate and Society (IRI)'s Climate Predictability Tool (CPT) (Meerbeeck, 2013). CCA is a multivariate regression relating patterns in predictor fields to patterns in the predictand field. An assessment by Bedward and Meerbeeck (2013) stated that the skill of the forecasts by the CIMH on the Caribbean is lowest for the Guianas, including Suriname. This could be related to the fact that the seasonal precipitation pattern of the Caribbean islands is different from that of Suriname. The Caribbean show a long rain season from May to November, with a short midsummer drought (Jul-Aug) and a dry season from December to April (Martinez et al., 2019).

According to the State of the Climate Report on Suriname (Solaun et al., 2021), the seasonal precipitation pattern in Suriname will and is undergoing change due to changes in the Inter Tropical Convergence Zone (ITCZ) seasonal cycle. It also states that the number of extreme events like prolonged drought periods, heavy precipitation events and accompanying flash floods and landslides are expected to increase in Suriname. This is possibly connected to a narrowing and strengthening of precipitation in the ITCZ (Byrne et al., 2018). The seasonality of precipitation characteristics in Suriname is mainly determined by the position and behaviour of the ITCZ (Fortuin et al., 2007). Understanding these climatic processes and their connections to precipitation patterns in Suriname is crucial for enhancing seasonal forecasting capabilities and improving our understanding of the region's climate variability. Investigating the teleconnections and relationships between boundary conditions and precipitation anomalies can provide valuable insights for improved forecasting, water resource management, and climate risk assessment in Suriname.

The predictors needed for seasonal forecasts vary per region around the world. In prior work on the precipitation regimes of Tropical South America the predictors highlighted by several studies are: The influence of the South American Monsoon System (SAMS), the South Atlantic Convergence Zone (SACZ), Atlantic Sea Surface Temperatures, the El Niño Southern Oscillation (ENSO) and the Inter Tropical Convergence Zone (ITCZ) (Córdova et al., 2022; Ferreira & Reboita, 2022). Tropical South America is a large and diverse area, spanning different areas such as the Amazon, and the Andes. The question therefore arises what the specific predictors for seasonal precipitation forecasts for Suriname are. Prior work focusing on Suriname, mainly looked into the relationship between precipitation variability in Suriname and the Atlantic SST anomalies and tropical Pacific ENSO SST anomalies (Nurmohamed et al., 2007). Other predictors of seasonal precipitation forecasts have not been thoroughly investigated for Suriname. The study by Nurmohamed et al. (2007) has looked into the

Sea Surface Temperature Anomalies (SSTA) predictors for the period 1961-1985. Since then numerous new data products have become available. This study can therefore add to the existing literature on Suriname by expanding both in the number of predictors as well as in the length of the time period of SSTA analysis.

The research objective of this study is to look into the sources of the predictive skill for seasonal precipitation forecasts for Suriname. To meet this objective, the following research questions were defined:

1. How accurate are gridded precipitation data sets, comprising interpolated observations, merged satellite-gauge and reanalysis) in displaying the precipitation characteristics in Suriname?
2. What are the characteristics of the historical seasonal precipitation pattern in Suriname, and its wet and dry composites?
3. What is the relation between sea surface temperature anomalies and precipitation anomalies in Suriname?
4. Where does the moisture that precipitates in Suriname originate from?
5. What can be said about the amount of predictive skill for Suriname of the predictors found?

This thesis report is structured as follows: Section 2 describes the study area. Section 3 provides a literature study on the potential drivers linked to precipitation anomalies in Suriname. In Section 4 the data and methodology of the research are described. Section 5 provides an overview of the results of this research. These results are discussed and related to prior literature, and recommendations for future studies are offered in Section 6. Section 7 concludes the research.

## 2 Study Area

This study focuses on Suriname and the surrounding area of French-Guiana and Guyana. Suriname lies in the Southern Caribbean or Tropical South America, next to the Atlantic Ocean. According to the Köppen climate system it has a Tropical rainforest (Af) and a Tropical monsoon (Am) climate (Peel et al., 2007). Around 80% of Suriname's surface is covered with rainforest. The remaining 20% are the northern coastal plains (Gersie et al., 2021), which can be seen in Figure 1.

The precipitation pattern in the study area is mainly determined by the natural movement of the Intertropical Convergence Zone (ITCZ), which traverses twice in north-south direction over Suriname. According to Naipal and Nurmohamed (2004) this results in the recognition of four seasons in the northern areas in Suriname; (1) the short wet season (begin December - begin February), (2) the short dry season (begin February - end April), (3) the large wet season (end April - mid August), and (4) the large dry season (mid August - begin December). In the southern part of Suriname there is only one wet and one dry season present (Antich-Homar et al., 2022). This difference between the north and south of Suriname can be illustrated by the position of the ITCZ, as seen in Figure 2. At the beginning of the year, the ITCZ is positioned to the south of Suriname, but still covering part of the country (Figure 2(a)). From April to August, the ITCZ moves northward and passes over Suriname, causing a long wet season (Figure 2(b)). During the second (long) dry season, the ITCZ lies to the north of Suriname (Figure 2(c)). Around December the ITCZ moves southward and passes Suriname for the second time (Figure 2(d)), resulting in the second short wet season, which continues into the short dry period for the north of Suriname and onto the wet period for the south of Suriname (Fortuin et al., 2007). Figure 1 illustrates that the divergent precipitation pattern, between the north and the south, is mirrored in the country's elevation as well. The low-lying terrain characterizes the northern coastal regions, while moving towards the southern part of the country, the elevation rises into the Guiana shield, reaching heights of just over 1000 meters above sea level (Solaun et al., 2021).

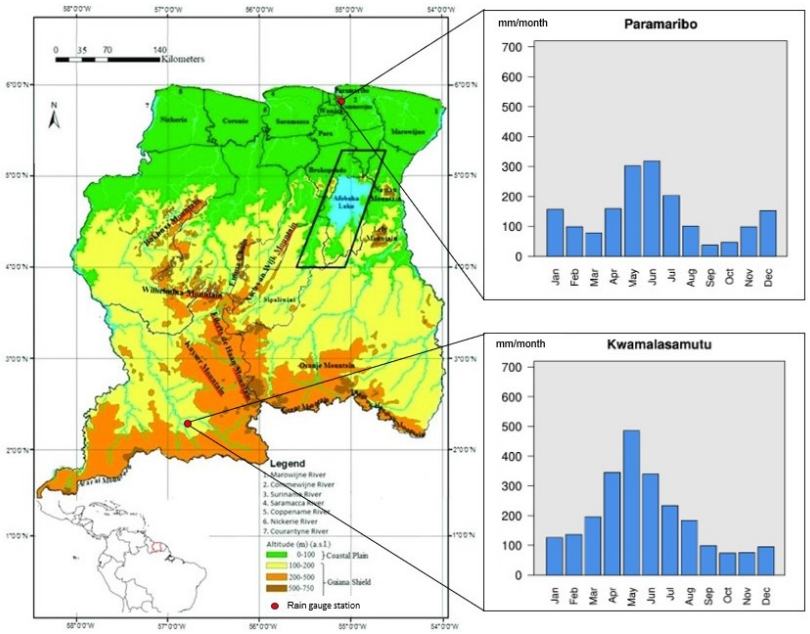


**Figure 1:** Topographic map of Suriname, showing elevation, retrieved from Gersie et al. (2021) and monthly accumulated precipitation for two locations averaged over the period 1990-2014 retrieved from Solaun et al. (2021).

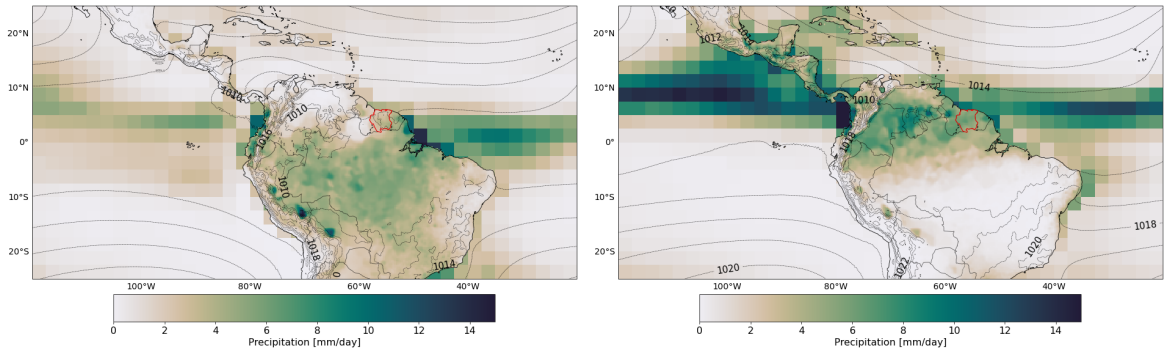


(a) February




(b) June

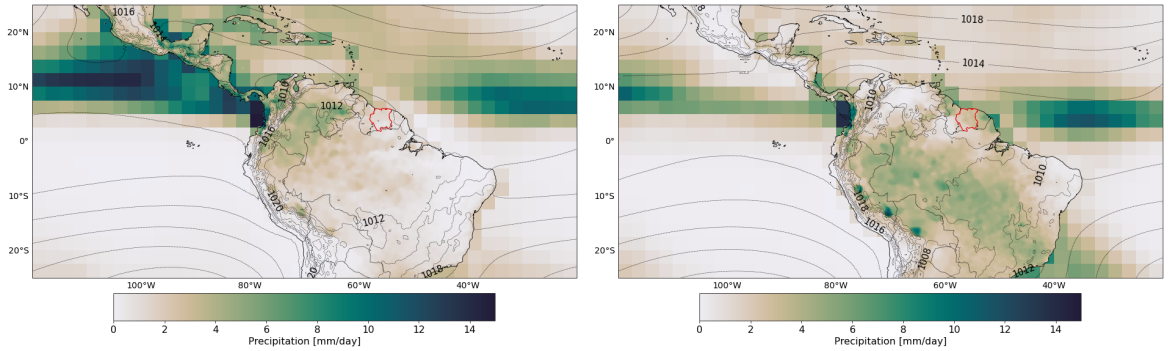


(c) September




(d) December

**Figure 2:** Movement of the ITCZ depicted by the mean precipitation values and mean Sea Level Pressure (SLP) over the period 1981-2020. Precipitation values are from the Global Precipitation Climatology Centre (GPCC) at 0.25° resolution over land and from the Global Precipitation Climatology Project (GPCP) at 2.5° resolution over the ocean combined. SLP is from the ERA5 reanalysis. The country area of Suriname is outlined with red.

# 3 Precipitation drivers of Suriname

As discussed in Section 2, the seasonal pattern of Suriname is primarily determined by the north-south movement of the ITCZ. However, successful seasonal forecasts rely on understanding the inter-annual climate variability, which entails deviations from the climatological average. The predictive skill of these anomalies on a seasonal timescale is connected to the more slowly evolving boundary conditions of the climate system, such as sea surface temperature (SST), soil moisture and snow cover. Anomalies within these boundary conditions are conveyed to the atmosphere through so-called "teleconnections." These teleconnections represent climatic connections between geographically separated regions (Kumar et al., 2020). The slowly varying boundary conditions are influencing weather patterns over long distances. The strength of these teleconnections can be assessed through the statistical correlation of fluctuations in relevant parameters.

Recent studies have identified key climatic processes associated with precipitation anomalies in Tropical South America. Córdova et al. (2022) found that the intensity and position of the South Atlantic Convergence Zone (SACZ), the meridional position of the ITCZ in relation to Atlantic Sea Surface Temperature (SST) anomalies, the El Niño Southern Oscillation (ENSO), and anomalies in the strength of the South American Monsoon System (SAMS) are primary drivers of precipitation anomalies. Similarly, Ferreira and Reboita (2022) highlighted the influence of the SAMS, SACZ, Atlantic SST, ITCZ and their interactions on the precipitation regimes of Tropical South America. These climatic processes are schematized in Figure 3 and will be discussed in the following sections.

## 3.1 ITCZ

The Intertropical Convergence Zone (ITCZ) represents the region of maximum tropical precipitation and corresponds to the ascending branch of the Hadley cell, where warm moist trade winds converge. Low pressure at the surface gives rise to vertical motion, deep convective cloud formation and precipitation. The mean position of the ITCZ is globally located around 5°N (Marshall et al., 2014) and this position has remained approximately constant over the past decades (Byrne et al., 2018). On a seasonal scale the position of the ITCZ shifts influenced by the amount of heat in the Northern Hemisphere (NH) versus the Southern Hemisphere (SH). During the boreal summer, the NH experiences atmospheric heating, while the SH undergoes atmospheric cooling. Consequently, the Hadley cell and the ITCZ shift northward toward warmer SSTs, placing the ITCZ approximately 9° north of the equator. In contrast, during the austral summer, the ITCZ shifts southwards towards the equator (Donohoe et al., 2013; T. Schneider et al., 2014). This inter-hemispheric temperature contrast influences seasonal precipitation patterns, with the ITCZ extending further towards the hemisphere with higher temperatures (T. Schneider et al., 2014). Regional ITCZ positions are dependent on continental configurations and local SST distributions (Marshall et al., 2014).

## 3.2 Atlantic Sea Surface Temperature

Sea Surface Temperature (SST) is one of the main boundary forcing mechanisms of the atmosphere. The oceans are a main driver of climate variability due to coupled ocean-atmosphere phenomena. Significant correlations between SST and precipitation observations have been found in the tropics (Dittus et al., 2018). Atlantic SST shows a clear seasonal pattern around the equator which is characterized by fast cooling during AMJJ, resulting in the formation of the equatorial Atlantic Cold Tongue (ACT) in JJA, and slower warming for the other months. The cooling (warming) is caused by strong southeasterly winds close to the equator producing upwelling (downwelling) and raise (deepen) the thermocline to the south (north) of the equator. The cooling enhances the contrast between warmer SST north of the equator and colder SST south of the equator (Cabos et al., 2019). This contrast in temperature is called the Tropical Atlantic Meridional Gradient (TAMG), which in its turn influences the position of the ITCZ. The main areas where behaviour of Tropical SST anomalies is measured in the Atlantic are: TNA (5.5N-23.5N, 15W-57.5W), TSA (0-20S, 10E-30W)and TAMG (TNA - TSA).

External factors that influence the Atlantic SST are ENSO and the North Atlantic Oscillation (NAO) (Mélice & Servain, 2003; Rodrigues et al., 2011).

### 3.2.1 Tropical Atlantic Variability

The Tropical Atlantic Variability (TAV) shows a clear seasonal and decadal variation consisting of three main modes; the Atlantic Zonal Mode (AZM), the Atlantic Meridional Mode (AMM) and the variability in the Angola-Benguela Front (ABF) in the southeastern tropical Atlantic (Cabos et al., 2019). The AZM or Atlantic Niño mode is controlled by equatorial ocean dynamics in response to surface winds, like ENSO in the Pacific, this is called the Bjerknes feedback (for more see Figure 4(b)). The Atlantic Niño is typically measured at (3°S–3°N, 0–20°W). The AMM is defined by a cross-equatorial gradient of SST anomalies, presented in Figure 4(a). During the positive (negative) phase of AMM, positive (negative) SST anomalies are seen north of the equator and negative (positive) SST anomalies south of the equator. Corresponding to these SST anomalies, the sea level pressure (SLP) anomalies are negative (positive) north of the equator and positive (negative) south of the equator (Cabos et al., 2019; Ríos-Cornejo et al., 2015). The main driving force behind the AMM is the Wind-Evaporation-SST (WES) feedback. The WES feedback mechanism involves a cross-equatorial atmospheric flow that reduces the strength of the trade winds in the warmer hemisphere and increases the strength of the trades in the cooler hemisphere (Amaya et al., 2017). This shift in trade wind strength contributes to the reinforcement of the meridional SST gradient. The meridional position of the Intertropical Convergence Zone (ITCZ) is found to be strongly related to these Atlantic Sea Surface Temperature (SST) anomalies (Córdova et al., 2022). During the positive (negative) phase of the AMM the ITCZ shifts further north (south) (Cabos et al., 2019).

## 3.3 South American Monsoon System

The South American Monsoon System (SAMS) is one of the major monsoon systems of the Southern Hemisphere and consists of a rainy season from November to March and a dry season from May to September (Marengo et al., 2012). The SAMS migrates together with the solar insolation cycle and is characterized by interaction between the topography of the South American continent and ocean-atmosphere dynamics (Martinez et al., 2019). During the rainy season one of the most important features of the SAMS for maintaining precipitation is the South Atlantic Convergence Zone (SACZ). The SACZ is characterized as a convective cloud band stretching from the Amazon region in the south-eastward direction, towards the Atlantic Ocean (Ferreira & Reboita, 2022). While Suriname does not directly lie in the region of the SACZ, it is likely to be influenced by the seasonal pattern of the SAMS. Taschetto and Wainer (2008) found that the SACZ is less predictable than the ITCZ, since it depends more on internal atmospheric variability while the ITCZ has a larger external dependence.

## 3.4 Pacific Sea Surface Temperature and El Niño Southern Oscillation

The El Niño Southern Oscillation (ENSO) is a coupled ocean-atmosphere phenomenon forcing SST patterns in the Pacific and thereby also the patterns of the ITCZ and SACZ. Episodes of ENSO consist of El Niño, with a warmer than usual east Pacific SST, and La Niña, with a colder than usual east Pacific SST. Appendix B shows a schematized picture of the Walker circulation during the boreal winter, when ENSO events are most pronounced. While atmosphere-ocean interactions of ENSO are centered in the equatorial Pacific Ocean, ENSO influences the global atmospheric circulation (Alexander et al., n.d.). Related to ENSO, SST anomalies develop in both the Pacific and Atlantic ocean. ENSO is also known to influence the position of the ITCZ; going from La Niña to El Niño conditions, the Pacific ITCZ shifts southward by about 2°, and during strong El Niño events by about 5° (T. Schneider et al., 2014).

The main areas where ENSO behaviour of SST anomalies are measured in the Pacific are: Niño 1+2: Extreme Eastern Tropical Pacific SST (0-10S, 90W-80W), Niño 3: Eastern Tropical Pacific SST (5N-5S, 150W-90W), Niño 3.4: East Central Tropical Pacific SST (5N-5S, 170W-120W), Niño 4: Central Tropical Pacific SST (5N-5S, 160E-150W)

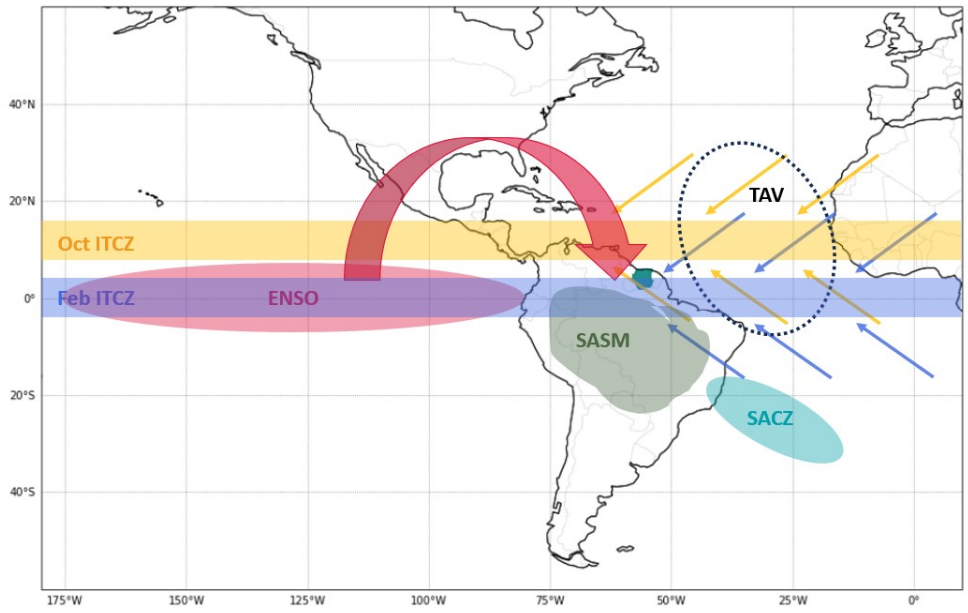


**Figure 3:** Schematic of precipitation drivers for Suriname. October position of the Inter Tropical Convergence Zone (Oct ITCZ); February Position of the Inter Tropical Convergence Zone (Feb ITCZ); El Niño Southern Oscillation (ENSO); South American Summer Monsoon (SASM); South Atlantic convergence Zone (SACZ) and Tropical Atlantic Variability (TAV). The country area of Suriname is colored in dark green.

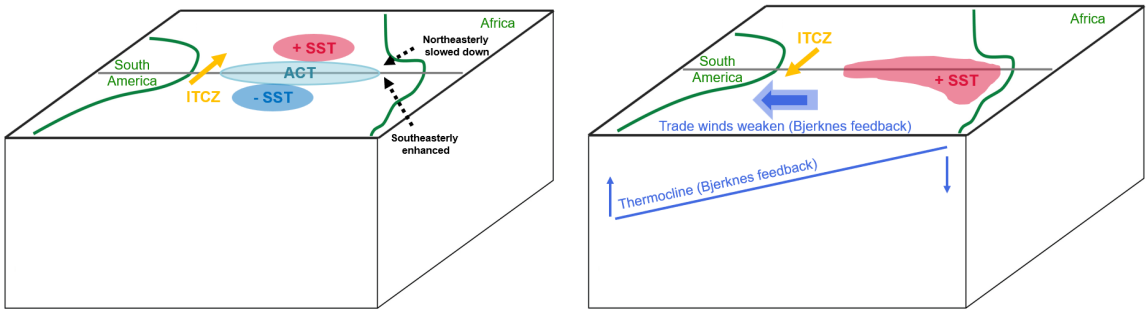


(a) AMM (b) AZM

**Figure 4:** (a) Schematic of processes during AMM positive mode. (b) Schematic of processes during AZM or Atlantic Niño. (Bjerknes feedback: When a small warming in the eastern Atlantic/Pacific causes the pressure gradient between the east and west to decline and the trade winds to weaken. This results in less upwelling of cold water in the eastern Atlantic/Pacific, which declines the thermocline. Because of this reduction in upwelling the waters in the east warm even more and further weaking of the trade winds cause El Niño.)

# 4 Materials and methods

This section describes the materials used within this study in Section 4.1, 4.2, 4.3 and 4.4 and the methods performed to answer the research questions in Section 4.5, 4.6, 4.7, 4.8, 4.9 and 4.10.

## 4.1 Gauge data

For the analysis of gridded precipitation data, multiple stations within Suriname were used. This data was obtained through the Latin America Climate Assessment & Dataset (LACA&D) and directly from the Meteorologische Dienst Suriname (MDS). Since the spatial density of gauge observations in Suriname varies within the time period 1950-2020, data from the neighbouring countries; Guyana and French-Guiana was also used. This data was obtained from the Koninklijk Nederlands Meteorologisch Instituut (KNMI) climate explorer, wich includes data from the Global Historical Climatology Network monthly version 2/3 (GHCNm). The station data from the LACA&D and MDS are of daily resolution, the KNMI climate explorer data is of monthly resolution. All data stations within Suriname are in the ownership of the MDS. The stations that are used in this research are summarized in Table 1 and the spatial spread of the stations is depicted in Figure 5.

**Data quality control:**

Prior to obtaining the data for this study the GHCNm stations have already been checked with a visual inspection, the time series were checked for changes in the mean, variance and scale, and every individual precipitation total was checked for outliers in space and time. The LACA&D stations were also checked for outliers and suspected values by the LACA&D itself. Missing and suspected values were flagged. For more detail on this quality control see appendix A. The flagged values of the LACA&D stations were removed.

An extra data quality control for the gauge data used in this study comprised of choosing only stations that had a consistent data period of at least 10 years and when multiple stations are in the same gridcel, the station that is of known good quality (defined by the MDS) was chosen over the station that is of unknown quality. During the resampling from daily to monthly data only months with 90% of complete gauge data are used, otherwise NaN values were given.

**Table 1:** Available rain gauge stations within Suriname, French-Guiana and Guyana.

| | Station name | Country | Source | Data period (used) | Location | Elevation |
|---|---|---|---|---|---|---|
| 1. | Groningen | Suriname | LACA&D | 1951-2000 | 5.80N, 55.47W | 0m |
| 2. | Cultuurtuin | Suriname | LACA&D | 1951-2000 | 5.85N, 55.17W | 2m |
| 3. | Georgetown | Guyana | GHCNm | 1951-2000 | 6.80N, 58.2W | 2m |
| 4. | Timehri | Guyana | GHCNm | 1951-2000 | 6.50N, 58.3W | 29m |
| 5. | Cayenne-Rochambeau | French-Guiana | GHCNm | 1951-2000 | 4.80N, 52.4W | 9m |
| 6. | Nickerie | Suriname | LACA&D, MDS | 1951-2022 | 5.95N, 57.03W | 4m |
| 7. | Zanderij | Suriname | LACA&D, GHCNm, MDS | 1951-2022 | 5.47N, 55.2W | 16m |
| 8. | Zorg en Hoop | Suriname | LACA&D, MDS, GHCNm | 1981-2022 | 5.82N, 55.2W | 3m |
| 9. | Saint Laurent | French-Guiana | GHCNm | 1981-2000 | 5.50N, 54.03W | 4m |
| 10. | Kuourou | French-Guiana | GHCNm | 1981-2000 | 5.30N, 52.8W | 14m |
| 11. | Saint Georges | French-Guiana | GHCNm | 1981-2000 | 3.88N, 51.8W | 2m |
| 12. | Marapasouila | French-Guiana | GHCNm | 1981-2000 | 3.63N, 54.03W | 104m |
| 13. | Kwamalasa-moetoe | Suriname | LACA&D, MDS | 1976-1986 + 2000-2022 | 2.35N, 56.8W | 750m |
| 14. | Sipaliwini | Suriname | LACA&D | 1976-1986 | 2.03N, 56.12W | 243m |
| 15. | Cottica | Suriname | MDS | 2006-2022 | 3.85N, 54.2W | 104m |
| 16. | Djoemoe | Suriname | MDS | 2006-2022 | 4.0N, 55.5W | 600m |

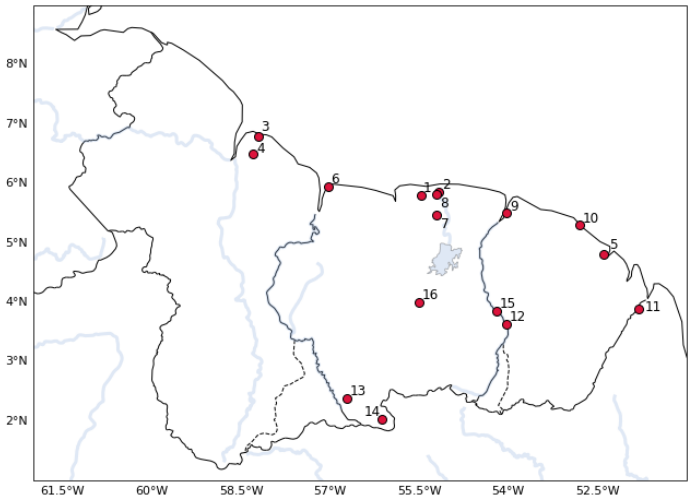


**Figure 5:** Spatial spread of the rain gauge locations of the stations that are included in this thesis report. Numbers correspond to Table 1.

## 4.2 Gridded precipitation data

In this study the Climatic Research Unit (CRU) TS v. 4.06, Global Precipitation Climatology Centre (GPCC) version 2022, Global Precipitation Climatology Project (GPCP) , Climate Hazards Group InfraRed Precipitation with Station data (CHIRPS), and ECMWF Re-Analysis v5 (ERA5) are used. An overview of the gridded precipitation datasets, hereafter GridPrecip, that were compared to station data can be found in Table 2. For further analysis in this thesis, the GPCC dataset was used. The foundation for this choice is presented in Chapter 5.1. Except for the moisture tracking, which is tailored to ERA5 data.

For certain parts of this thesis a mean value of precipitation for Suriname was used, this value was calculated by taking the weighted mean of the gridcells that fall within the box between 1°N-7°N latitude and 59°W-53°W longitude. Except for the moisture tracking analysis where the weighted mean within a shapefile of the Suriname country borders was taken.

**Table 2:** Gridded precipitation data sets that were used in this thesis report.

| Data set | Data type | Temporal resolution | Spatial resolution | Reference |
|---|---|---|---|---|
| CRU | Interpolated observations | Monthly(1901-2021) | 0.5°x0.5° | (Harris et al., 2020) |
| GPCC | Interpolated observations | Monthly (1891-2020) | 0.25°x0.25° | (U. Schneider et al., 2022) |
| GPCC daily | Interpolated observations | Daily (1982-2020) | 1.0°x1.0° | (Ziese et al., 2022) |
| GPCP | Merged satellite-gauge | Monthly (1979-present) | 2.5°x2.5° | (Adler et al., 2003) |
| CHIRPS | Merged satellite-gauge | Monthly (1981-present) | 0.05°x0.05° | (Funk et al., 2015) |
| ERA5 | Reanalysis | Daily (1950-present) | 0.25°x0.25° | (Hersbach et al., 2020) |

## 4.3 Predictor data

For the connection between the drivers of precipitation and the seasonal precipitation anomalies the data sets listed in Table 3 are used.

**Table 3:** Gridded predictor data sets that were used in this thesis report.

| data set | Variable | Data type | Temporal resolution | Spatial resolution | Reference |
|---|---|---|---|---|---|
| HadISST | SST | Interpolated observations | Monthly (1871-present) | 1.0°x1.0° | (Rayner et al., 2003) |
| ERA5 | W500, V10, U10, V850, U850, V200, U200, SLP | Reanalysis | Monthly (1950-present) | 0.25°x0.25° | (Hersbach et al., 2020) |
| ERA5 | U10, V10, tp , sp, e, tcw, precip and on pressure levels: u, v, q | Reanalysis | Hourly (1950-present) | 0.25°x0.25° | (Hersbach et al., 2020) |

## 4.4 Software and tools

All the computations were carried out on the Dutch national e-infrastructure with the support of SURF Cooperative. Calculations were done with Python3 v3.9.16 (Python3) and Climate Data Operators (CDO).

## 4.5 Statistics

Several statistical equations and methods were used in this thesis report, which are described in this section.

**Precipitation data quality check**

Following the studies of Ayoub et al. (2020), Satgé et al. (2020), Schumacher et al. (2020), Ahmed et al. (2019), and Nogueira (2020) on the comparison of observations and gridded precipitation data sets in other regions of the world the following statistics were applied:

- Mean ($\mu$)
- Monthly climatology and anomalies to the monthly climatology
- Root mean square error (RMSE)
- Spearman correlation ($r_s$)
- Mean error (BIAS)

With these statistics the central tendency (Mean and Median), the dispersion (Standard deviation and RMSE) and dependence (Spearman correlation) of the data can be analyzed.

The positive bias values indicate an underestimation by the gridded set (too little precipitation predicted) and the negative bias values indicate an overestimation by the gridded set (too much precipitation predicted).

**Table 4:** Statistical measures. ($O_i$, observations; $P_i$, gridded precipitation; N, number of data pairs; R, Rank.

| Name | Equation | Perfect score |
|---|---|---|
| Spearman correlation ($r_s$) | $\frac{cov(R(O_i),R(P_i))}{\sigma_{R(O_i)}\sigma_{R(P_i)}}$ | 1 (or -1) [-1,1] |
| Root Mean Squared Error (RMSE) | $\sqrt{\frac{1}{N}\sum(O_i - P_i)^2}$ | 0 |
| Mean error (BIAS) | $\frac{1}{N}\sum(P_i - O_i)$ | 0 |

**Spearman correlation:**

The Spearman correlation is a measure of rank correlation. It describes the strength and direction of the relationship between the SSTA and precipitation anomalies using a monotonic function. This is the ratio between the ranked covariance and the ranked product of standard deviations, with perfect scores at -1 and 1.

The Spearman rank correlation focuses on the order of values rather than their exact magnitudes. This is suitable for the relation between SST and precipitation data, since the relationship does not have to be linear. It captures monotonic relationships, where the variables tend to move together in the same direction (either increasing or decreasing) without assuming a specific form of the relationship. Also the Spearman correlation is more suitable for precipitation data than for instance the Pearson correlation, because it is less sensitive to outliers in the data.

**Significance**

To give extra information on every correlation performed, the significance of that correlation was also calculated. This is done by performing the Student's t-test and calculating the corresponding p-value, which can be applied in this study since the sample size is large enough.

$$t* = \frac{\overline{x} - \mu}{\sigma/\sqrt{n}} \tag{1}$$

For this thesis report a two-sided t-test with two degrees of freedom was performed and a correlation was considered significant when $p \leq 0.05$.

## 4.6 Analysis of gridded precipitation sets in comparison to gauge data

Since there are not enough long, recent time series of rain gauges that can cover the whole area of Suriname, GridPrecip's were evaluated on their quality of spatial and temporal performance over Suriname, in order to use these sets for later steps in the research. For the aim of this study the station data is (after a small quality check) adopted as true. Nevertheless, the comparison made can also be viewed as an objective comparison between both the gridded precipitation datasets and the station data.

The period for the main analysis (1981-2000) was chosen based upon the fact that;

- 1981 is the first year in which all GridPrecip are available.
- There were only 5 stations with data after the year 2000.
- 20 years is a period long enough to cover different climatic conditions and to perform this analysis. According to World Meteorological Organization (2011) 5 years is already sufficient.

A total of 11 stations that are therefore used for the main analysis of all the GridPrecip for the time period 1981-2000 are presented in Figure 6(a). As can be seen in Figure 6(a) the stations for the period 1981-2000 do not cover the inner or southern part of Suriname, therefore the period 1976-1986

was also chosen for the analysis between the northern and southern parts of Suriname. This analysis was performed between 6 stations and the CRU, GPCC and ERA5 sets (Figure 6(b)). The period 1952-2000 was chosen for an extended time period analysis between 7 stations and the CRU and GPCC datasets (Figure 6(c)). This was carried out to confirm whether the analysis had produced an incorrect high score for these sets, due to the fact that these GridPrecip comprise interpolated station data, and the analysis was a point-to-grid comparison. For CRU it is known which stations are included in the set (see Table 5). For GPCC the information available shows only how many stations are incorporated in a gridcel. See Appendix D. Finally, the more recent period of 1999-2018 was used to compare three stations with CHIRPS, CRU, ERA5, GPCC and GPCP (Figure 6(d)).

Since the spatial density of gauge observations is low in Suriname the comparison was done point-to-grid, where precipitation observed at a station was compared to the GridPrecip of the corresponding gridcel. All data sets are plotted in their native spatial resolution except for CHIRPS which was regridded from 0.05 to 0.25 for calculation purposes.

To assess the quality of gridded observational and reanalysis data sets in displaying the precipitation characteristics in Suriname, the following precipitation characteristics were chosen; the long-term average (climatology), monthly and yearly anomalies to the climatology (obtained by subtracting the climatology from the timeseries) and seasonal composites.

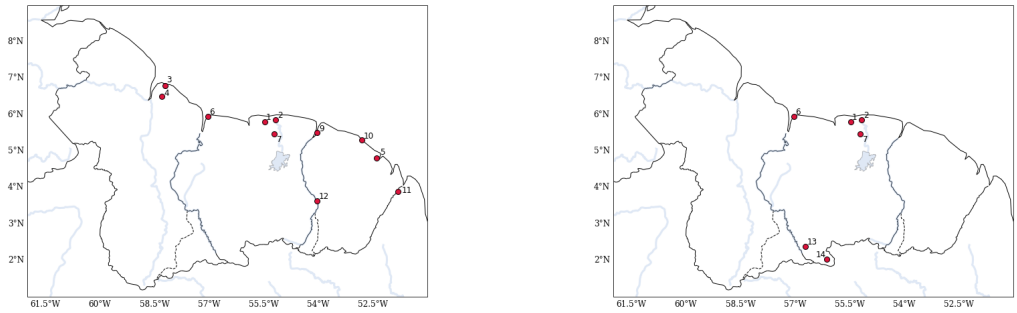


(a) 1981-2000

(b) 1976-1986

(c) 1952-2000

(d) 1999-2018

**Figure 6:** Location of stations that are used for the comparison of GridPrecip with rain gauge data for certain time periods: (a) 1981-2000 (b) 1976-1986 (c) 1952-2000 (d) 1999-2018

**Table 5:** The stations (used within the analysis 1981-2000) that are and are not included within the CRU dataset.

| Station Name | Country | Location | Included in CRU |
|---|---|---|---|
| Georgetown | Guyana | 6.8N 58.15W | Yes |
| Zanderij | Suriname | 5.45N 55.2W | Yes |
| Saint-Laurent | French-Guiana | 5.5N 54.03W | Yes |
| Maripasoula | French-Guiana | 3.63N 54.03W | Yes |
| Saint Georges | French-Guiana | 3.88N 51.8W | Yes |
| Nickerie | Suriname | 5.95N 57.03W | Yes |
| Cultuurtuin | Suriname | 5.83N 55.15W | Yes |
| Cayenne-Rochambeau | French-Guiana | 4.80N 52.4W | No |
| Groningen | Suriname | 5.79N 55.48W | No |
| Timehri | Guyana | 6.50N 58.30W | No |
| Kuourou | French-Guiana | 5.30N 52.80W | No |

## 4.7 Definition of the seasons

Due to the contrasting weather patterns in Suriname (the coastal region in the north experiences four seasons, while the inland region in the south only has two seasons) a different definition of the seasons was made.

Typically, the wet and dry seasons are generally defined as the values that fall above and below the mean. In Figure 7 it can be seen that for Suriname this results in a wet season spanning the months April, May, June and July (AMJJ) and a dry season covering the months August, September, October and November (ASON). The months of December, January, February and March (DJFM) fluctuate around the mean and are therefore named the in-between season. For this analysis, the four previously mentioned seasons were not considered; instead, the short wet and short dry seasons were combined into a single "in-between season."

For the definition of the seasons, the 30 day running mean of the GPCC dataset was used, as it provides data on a daily basis. The initial differentiation of the seasons was made upon a daily basis, but translated to whole months.

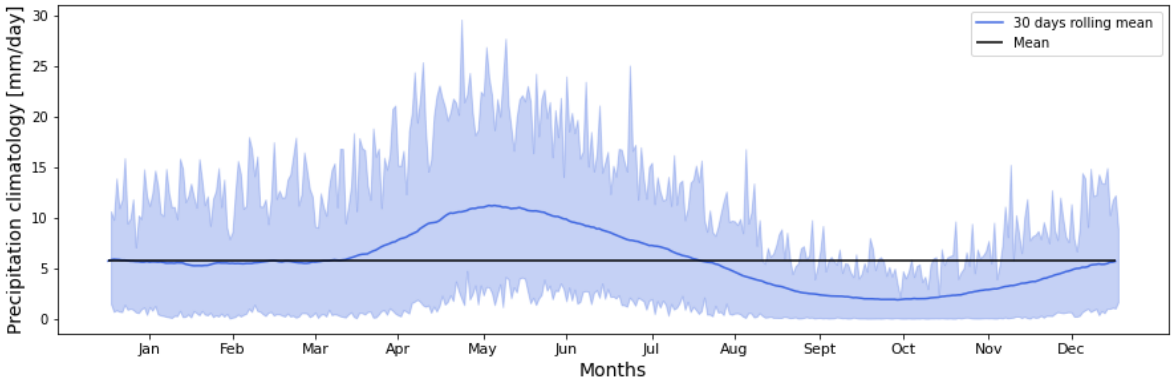


**Figure 7:** Climatology of the 30-day running mean precipitation [mm/day], for the period 1981-2020, over Suriname. Including the band of precipitation between the 90th and 10th percentile. Data from the Global Precipitation Climatology Centre (GPCC).

## 4.8 Sea surface temperature correlation

Correlation maps between precipitation anomalies and sea surface temperature anomalies (SSTA's) were calculated.

### Data set pre-processing

For the correlation of the monthly spatial average precipitation over Suriname versus monthly SSTA's both the SST and the precipitation were detrended with CDO from there long term trend (1950-2020) as seen in Figures 8 and 9. The SST values were detrended per gridcell and the spatial precipitation average was detrended. This long term trend was calculated by a linear regression least-squares method;

$$y = \alpha + \beta X \tag{2}$$

Where $\beta$ denotes the rate of change or trend over the selected time period.

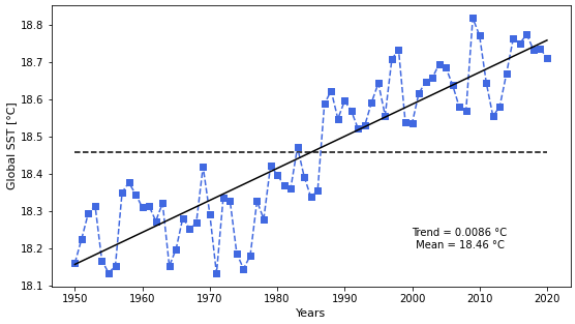


**Figure 8:** Timeserie of yearly values of the global average SST [°C] for the timeperiod 1950-2020, including the mean value and trend over this period. Data from HadISST.

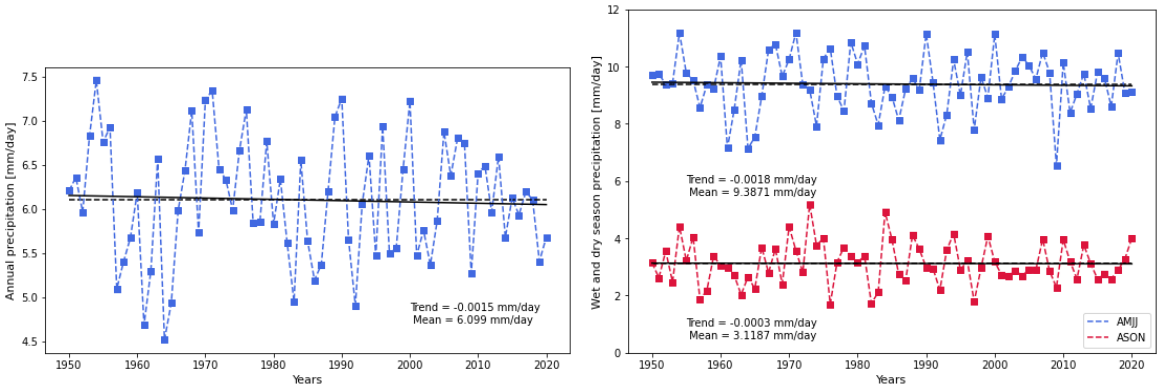


(a) Annual

(b) AMJJ and ASON season

**Figure 9:** Timeserie of yearly values of the average precipitation within Suriname [mm/day] for the timeperiod 1950-2020, including the mean value and trend over this period. Data from Global Precipitation Climatology Centre (GPCC).

Both SST and precipitation anomalies were obtained by subtracting the longterm monthly average (1950-2020) from the total time series. The spatial average of Suriname precipitation anomalies was than compared to the SSTA at every gridcel. To perform the spatial correlation by CDO the anomalies to the precipitation average over Suriname were enlarged to the same grid as the SSTA (1.0° by 1.0°).

Both an annual correlation and a seasonal correlation was performed. These regions (Pacific index 1 and 2) were used as an index, comprised of the spatial average of the SSTA. The annual correlation was computed by correlating monthly anomalies for the entire timeserie of 1950-2020 on every gridcell.

Per gridcell, this is 71 years times 12 months is 852 values. Also a seasonal correlation was performed. Per gridcell, this is 71 years times 4 months is 284 values. For reference also a monthly correlation was performed, but since this consists of a lower number of data the significance is also lower.

### Indices

From the created correlation maps regions of high correlation between the anomalies were determined. Together with SSTA indices that were used in prior literature (Nurmohamed et al., 2007; van Oldenborgh et al., 2021), the spatial average SSTA's over these index areas were correlated against precipitation anomalies over Suriname. The index areas are shown in Figure 10.

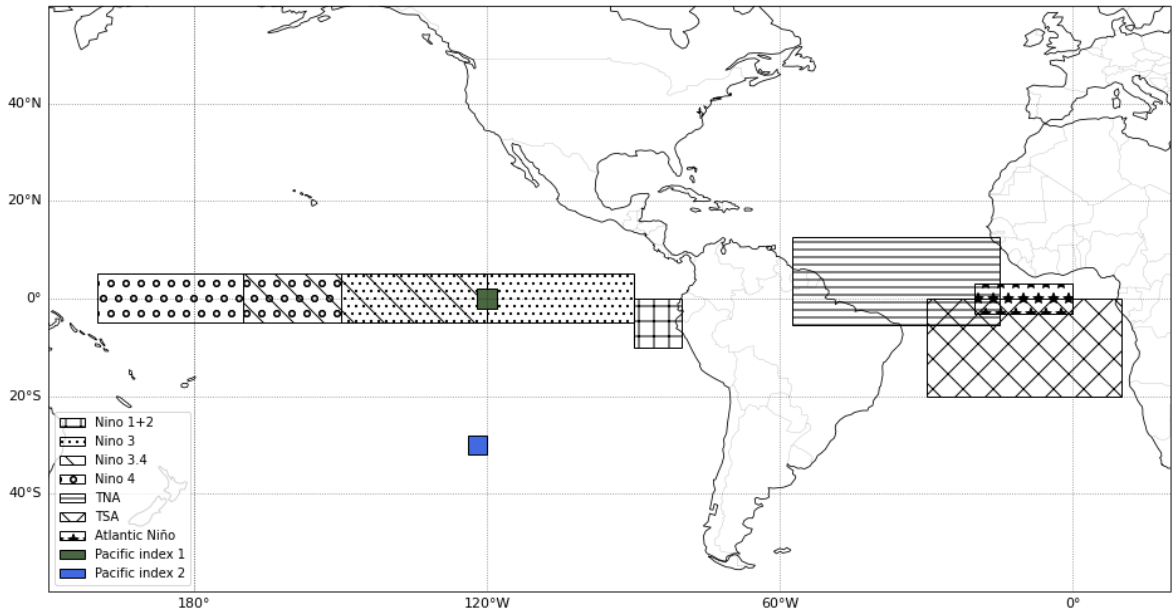


**Figure 10:** The location of SST indices used in this thesis report.

### Regression

Linear regression maps were also calculated between precipitation anomalies and SSTA's. On the same detrended series of SSTA and precipitation anomalies a linear least-squares regression was performed, resulting in maps of the slope of the linear regression (ΔPrecipitation [mm/d] / ΔSST [°C]).

## 4.9 Composites

To analyze the deviations from the mean climatology, composites of wet and dry periods were made. This was done with the use of the Standardized Anomaly Index (SAI). Standardized anomalies offer more information about the magnitude of the anomalies, due to the removal of dispersion by dividing by the climatological standard deviation. This rainfall-based index is used by multiple studies to analyze the variability of rainfall (Gao et al., 2022; Koudahe et al., 2017; Reboita et al., 2021). The SAI is expressed as:

$$SAI = \frac{(X_i - \mu)}{\sigma}, \tag{3}$$

where $X_i$ is the rainfall in a specific period $i$ (e.g., monthly, seasonal, or annual), $\mu$ is the mean value over a period of observation, $\sigma$ is the standard deviation of the rainfall over a period of observation, which represents the variability or spread of the data.

By dividing the deviation $(X_i - \mu)$ by the standard deviation $(\sigma)$, the SAI expresses the anomaly in terms of standard deviations from the mean. A positive SAI indicates that the observed value is above the mean, while a negative SAI indicates that the observed value is below the mean. Years above the

threshold of one standard deviation (SAI≥1) are considered to be severely wet and years below one standard deviation (SAI≤-1) are considered to be severely dry.

To obtain the wet and dry composites per season, the monthly values of the seasons were separated for all three seasons (DJFM, AMJJ and ASON). The SAI values were then calculated by using the mean value of each season for the period of 1950-2020, shown in Figure 11.

The composite years used for the moisture tracking analysis are listed in Table 6. The downloading of ERA5 data for the use in the moisture tracking model (WAM2layers) was very time intensive, therefore only the three most recent composite years for every season were chosen. The choice of the most recent years and not the most extreme composites is based upon the fact that the ensemble spread of ERA5, and therefore the uncertainty in the quality of the data, becomes larger when data further back in time is chosen (Hersbach et al., 2020).

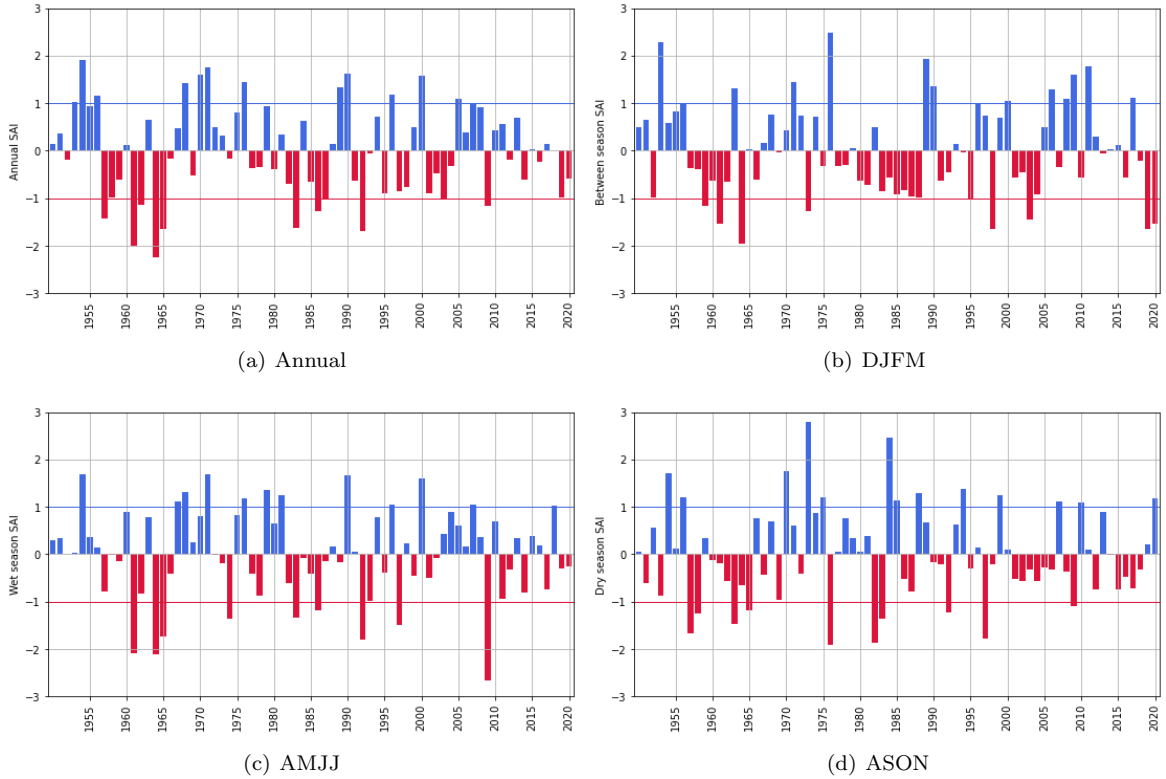


(a) Annual (b) DJFM

(c) AMJJ (d) ASON

**Figure 11:** Standardized Anomaly Index (SAI) of Suriname precipitation with reference to the 1950-2020 average. (a) Annual; (b) December-January-February-March (DJFM); (c) April-May-June-July (AMJJ) (d) August-September-October-November (ASON).

**Table 6:** Composites that are used for the moisture analysis.

| Season | Wet composite | Dry composite |
|---|---|---|
| DJFM | 2009, 2011, 2017 | 2003, 2019, 2020 |
| AMJJ | 2000, 2007, 2018 | 1992, 1997, 2009 |
| ASON | 2007, 2010, 2020 | 1992, 1997, 2009 |

## 4.10 Moisture tracking

For the backtracking of moisture that precipitated in Suriname the WAM2-layers model of Van Der Ent et al. (2022) was used. The full code is provided on the GitHub repository and a short summary is given below, for indepth information see Van Der Ent et al. (2014).

WAM2-layers is an Eulerian moisture tracking model that can track the precipitation within a certain source region back to the evaporation source areas or track the evaporation within a certain source region forward to the precipitation areas. The model is based upon the water balance, which is solved for each gridcell and each timestep within the model:

$$\frac{\partial S_k}{\partial t} = \frac{\partial (S_k u)}{\partial x} + \frac{\partial (S_k v)}{\partial y} + E_k - P_k + \xi_k \pm F_v[L^3 T^{-1}], \tag{4}$$

where $S_k$ is the atmospheric moisture storage in layer $k$, $t$ is time, $u$ and $v$ are the wind components in $x$ (zonal) and $y$ (meridional) direction, $E_k$ is evaporation entering layer k, $P_k$ is precipitation removed from layer k, $\xi$ is a residual and $F_v$ is the vertical moisture transport.

For this research it was used for the backtracking of where precipitation originally evaporated by calculating the moisture transport between grid cells. The input needed to run WAM2layers is the 10m wind speed in both directions ($u$- and $v$-component), the u- and v-component of the wind at multiple (pressure) levels, humidity at multiple (pressure) levels, the 2m dewpoint temperature, the surface pressure, evaporation at the surface, the total column water and precipitation from a defined region, all from ERA5. The ERA5 data is acquired with the help of a CDS API key from the ERA5 database. The data was downloaded directly in the correct NetCDF format of 22 modellevels with a spatial resolution of 0.25x0.25, covering the area of 45N to 45S latitude by 90W to 20E longitude, and a temporal resolution of one hour. In Figure 12 the region of interest for the moisture tracking is shown. The precipitation that is backtracked originates from within the shapefile of Suriname and is tracked throughout the whole region of interest, confined by (45N, -90W, -45S, 20E).

Moisture recycling can be defined in multiple ways. In this report the regional precipitation recycling and continental precipitation recycling as defined by Van Der Ent et al. (2010) were used.

Regional precipitation recycling ($\rho_r$) is the amount of precipitation falling in a region which originates from evaporation within that same region, here the country of Suriname.

$$\rho_r = \frac{P_r}{P} \tag{5}$$

Continental precipitation recycling ($\rho_c$) is the amount of precipitation falling in a region which has evaporated from a continental area instead of an oceanic region. In this research the continental area is confined to South America.

$$\rho_c = \frac{P_c}{P_o + P_c} \tag{6}$$

The evaporation recycling ratio is the amount of tracked evaporation that ends up precipitating over Suriname originating over Suriname.

$$e_r = \frac{E_r}{E} \tag{7}$$

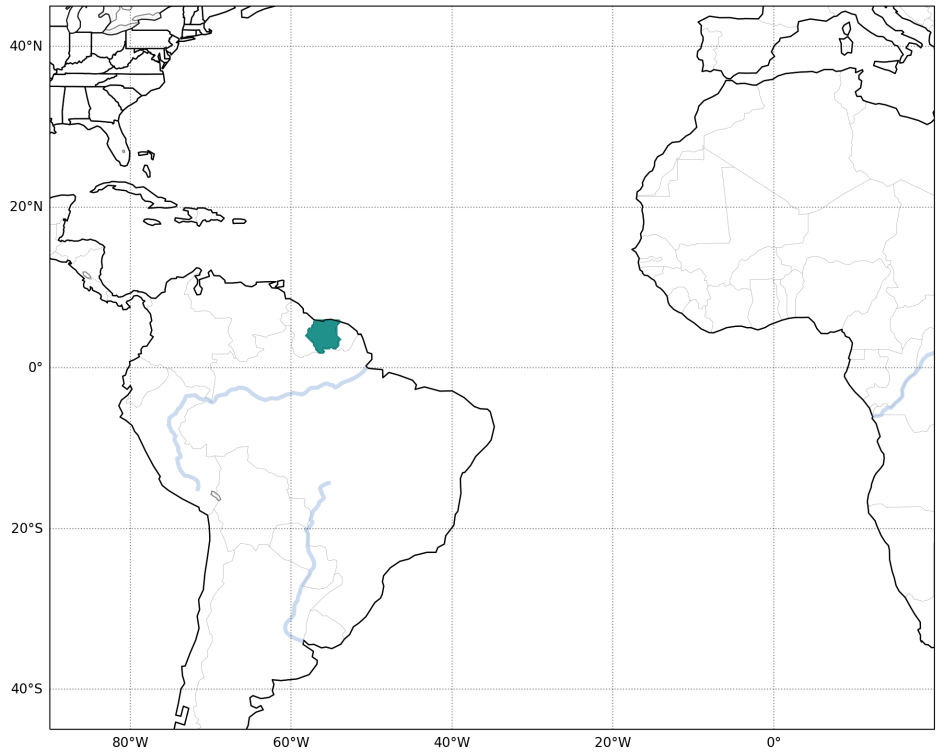


**Figure 12:** Region of interest for moisture tracking with WAM2layers. Source region of Suriname in green.

# 5 Results

This section describes the findings of this study in the order of the first four research questions that were formulated in Section 1. Starting with an analysis of five gridded precipitation sets (GridPrecip) in comparison to station gauge data (Section 5.1), followed by the characteristic of historical precipitation for the seasons in Suriname (Section 5.2). Section 5.3 then shows the results of Sea Surface Temperature correlations with precipitation anomalies in Suriname followed by the moisture tracking results of precipitation in Suriname in Section 5.4.

## 5.1 Spatial and temporal analysis of gridded precipitation sets in comparison to gauge data

Five GridPrecip (CRU, GPCC, ERA5, GPCP, CHIRPS) are compared to station gauge data with a point-to-grid comparison.

**Intercomparison of the five selected GridPrecip averaged over the Suriname area**

Averaged over the entire Suriname area, all GridPrecip follow the same seasonal pattern. In absolute monthly precipitation values ERA5 differs the most of all five sets, both in the monthly time series as in the climatology. For the period 1981-2000 and the more recent period 2001-2020 the annual climatological cycles of all data sets are presented in Figure 13 and Figure 14. In the driest months (ASON) the mean monthly precipitation is around 2-4 mm/d and in the wettest months (AMJJ) around 8-12 mm/d. For the period 1981-2000 ERA5 is showing drier conditions for almost all months compared to the other sets. The other sets agree fairly well (within 1 mm/d) for the second half of the year, but show more spread (up to 2 mm/d) in the earlier months of the year (DJFM season and the onset of the AMJJ season). In the period 2001-2020 the sets are closer together, but in the months January, February and March ERA5 and GPCP show a drier pattern than the other sets. CHIRPS and CRU show a larger peak in precipitation in May. Overall the data sets show a similar climatological pattern with the same seasonal pattern.

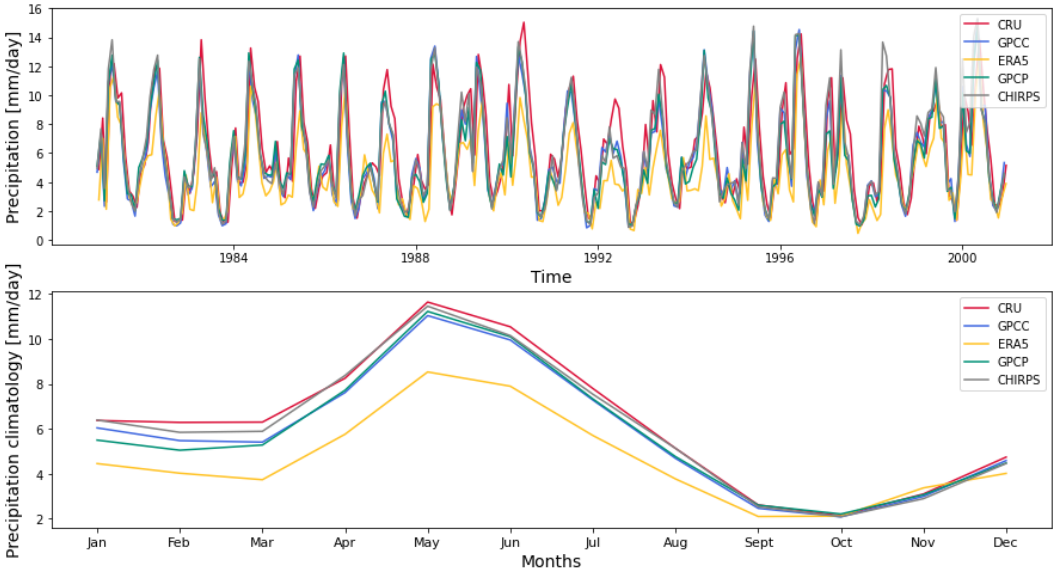


**Figure 13:** Mean precipitation of GridPrecip values (CRU, ERA5, CHIRPS, GPCC, GPCP) over Suriname area for the period 1981-2000. (above) entire time series (below) climatology.

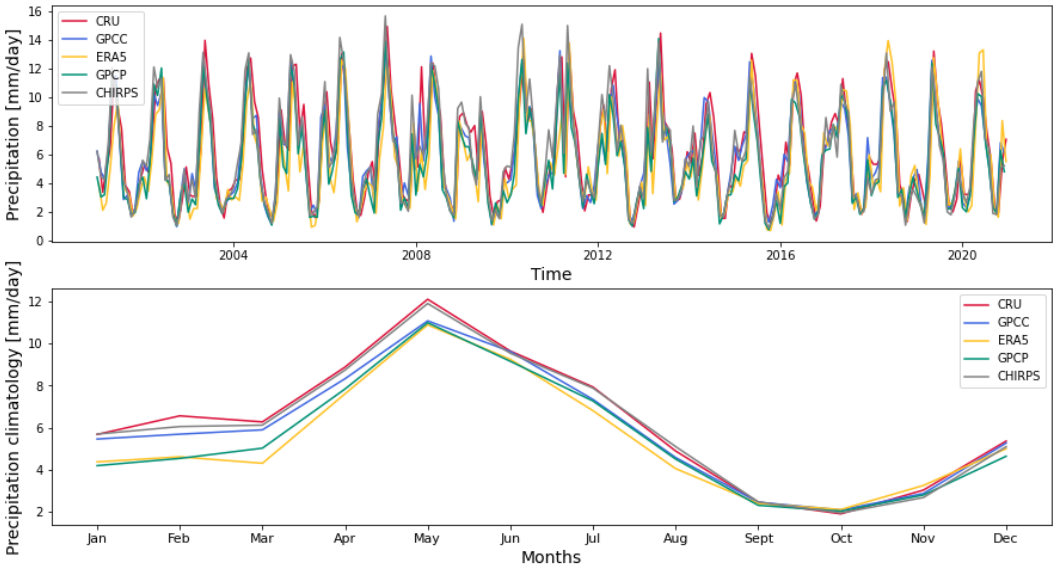


**Figure 14:** Mean precipitation of GridPrecip values (CRU, ERA5, CHIRPS, GPCC, GPCP) over Suriname area for the period 2001-2020. (above) entire time series (below) climatology.

### 5.1.1 Main analysis 1981-2000

For the period 1981-2000 the five GridPrecip are compared to 11 stations on a point-to-grid basis. The statistics and findings of this period are presented in this section.

**Accuracy of annual precipitation**

Compared to station Cultuurtuin all GridPrecip follow a similar anomalous annual pattern; large anomalies, corresponding to distinct wet and dry years are of the correct sign (positive or negative) and magnitude. However small anomalies fluctuate around zero. In Figure 15 are the annual anomalies presented of the gridded sets compared to the precipitation of station Cultuurtuin. The difference between dry and wet years is overall well captured by the gridded sets. There is no set that clearly captures the dry and wet year anomalies best. Every year another set is closest in precipitation amount to station Cultuurtuin. The overall performance of all GridPrecip individual on an annual basis is therefore less accurate than all the GridPrecip combined.

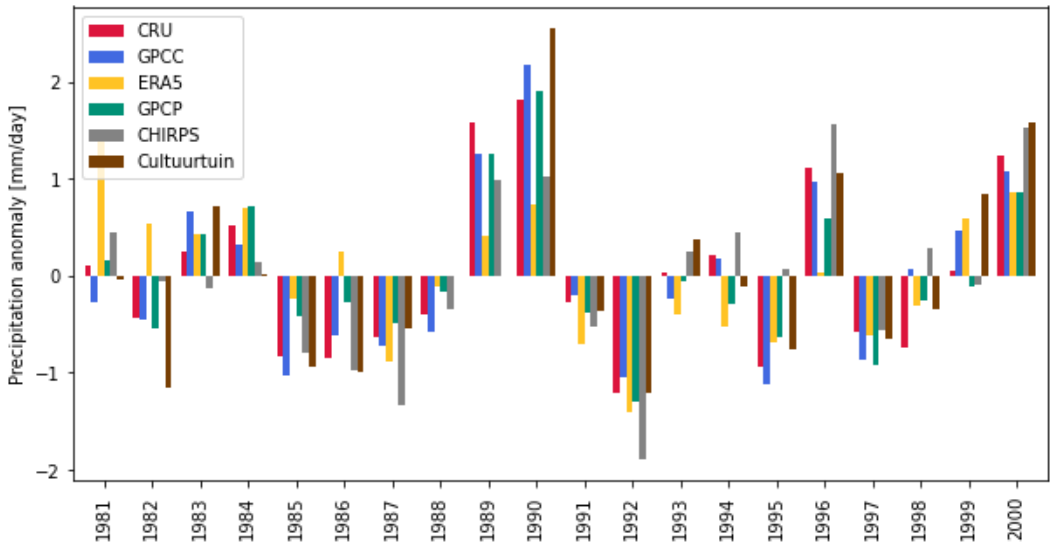


**Figure 15:** Annual anomalies for the GridPrecip values (CRU, ERA5, CHIRPS, GPCC, GPCP) at the location of station Cultuurtuin for the period 1981-2000.

### Accuracy of monthly and seasonal precipitation

On point-to-grid basis all GridPrecip are compared to station gauge data with Spearman rank correlation, RMSE and bias. GPCC shows the best statistical results of the five sets for this analysis. All measured statistics are combined into Table 7. Here it is shown that averaged over all stations GPCC scores best on both correlation between monthly mean and monthly anomalies to the climatology, and on RMSE. CHIRPS scores best on monthly bias averaged over all the stations versus GridPrecip. However when taking a look on the individual gauge comparisons (e.g. station Cultuurtuin and Zanderij in Figure 16) CHIRPS shows large differences to the gauge data (4 mm/d), and the low bias values are due to the average that is taken. In general all the GridPrecip show an annual dry bias; meaning that the gridded sets show a value of precipitation that is lower than the observed value in the stations.

All sets follow the climatology pattern of the stations. In Figure 16 the precipitation climatology of the stations Cultuurtuin and Zanderij are plotted against the GridPrecip for the location of that grid cell. The pattern is similar for all sets. In the dry season all sets behave similar to the station data. During the in-between season there is more spread, with CRU slightly overestimating, but behaving best. In the wet season GPCC and GPCP are closest to the Cultuurtuin precipitation values and GPCC and CRU are closest to the Zanderij precipitation values. Compared to Station Cultuurtuin all GridPrecip are within 1 mm/day difference for the months JASON. In the other months, CRU, CHIRPS, GPCC and GPCP differ up to 1.5 mm/day and ERA5 even up to 3 mm.day in Jan. Compared to Station Zanderij the GridPrecip, except CHIRPS, are within 2 mm/day difference for the entire year. CHIRPS differs up to 4 mm/day in May and June.

**Table 7:** Average statistics between the GridPrecip sets and observations over the 1981-2000 period. Bold score is the best scoring GridPrecip set for that statistic and season.

| | Dataset | Spearman monthly | Spearman anomalies | RMSE monthly (mm/d) | Bias monthly [mm/d] |
|---|---|---|---|---|---|
| Annual | CRU | 0.88 | 0.76 | 2.29 | 0.15 |
| | ERA5 | 0.79 | 0.61 | 3.5 | 1.4 |
| | GPCC | **0.93** | **0.88** | **1.5** | 0.40 |
| | GPCP | 0.85 | 0.70 | 2.8 | 0.66 |
| | CHIRPS | 0.87 | 0.75 | 2.4 | **0.073** |
| AMJJ | CRU | 0.82 | 0.74 | 2.6 | **0.13** |
| | ERA5 | 0.65 | 0.58 | 4.3 | 2.0 |
| | GPCC | **0.91** | **0.89** | **1.6** | 0.50 |
| | GPCP | 0.76 | 0.67 | 3.3 | 0.74 |
| | CHIRPS | 0.81 | 0.74 | 2.9 | 0.21 |
| ASON | CRU | 0.79 | 0.68 | 1.7 | 0.52 |
| | ERA5 | 0.67 | 0.57 | 2.1 | 0.19 |
| | GPCC | **0.85** | **0.82** | **1.3** | 0.322 |
| | GPCP | 0.78 | 0.67 | 1.8 | 0.27 |
| | CHIRPS | 0.78 | 0.69 | 1.6 | **0.096** |
| DJFM | CRU | 0.81 | 0.82 | 2.3 | -0.15 |
| | ERA5 | 0.67 | 0.68 | 3.7 | 1.9 |
| | GPCC | **0.91** | **0.91** | **1.4** | 0.38 |
| | GPCP | 0.77 | 0.77 | 2.9 | 0.98 |
| | CHIRPS | 0.80 | 0.80 | 2.4 | **-0.058** |

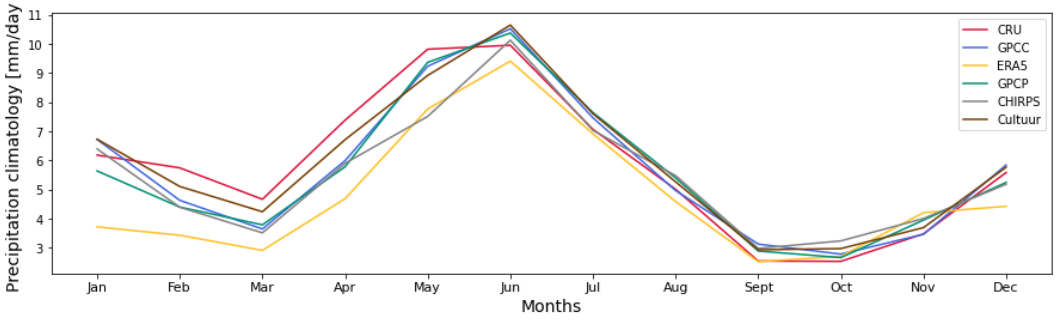


(a) Cultuurtuin

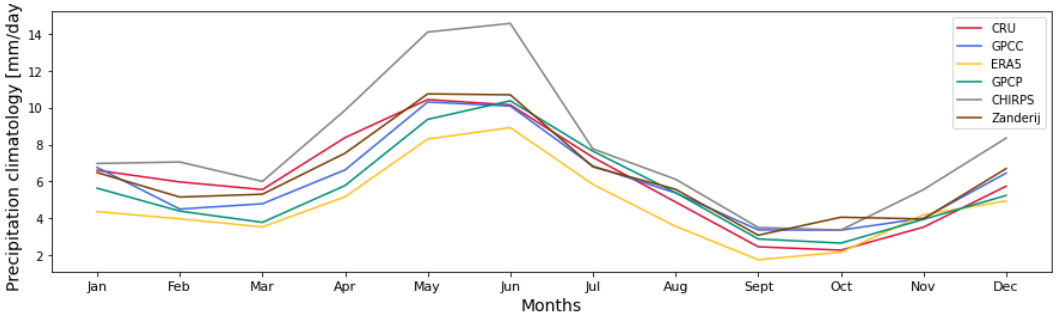


(b) Zanderij

**Figure 16:** Mean precipitation at the location of station (a) Cultuurtuin (b) and Zanderij for the period 1981-2000. Showing both the gauge data from station Cultuurtuin and Zanderij as well as the GridPrecip values (CRU, ERA5, CHIRPS, GPCC, GPCP) of the gridcell located at the location of station Cultuurtuin and Zanderij.

### Accuracy of spatial distribution

The spatial patterns for CRU, CHIRPS and GPCC are similar in their distribution of wetter and drier areas, ERA5 shows an overall drier pattern. The grid of GPCP is a lot coarser and therefore the set is spatially hard to compare to the other sets. In Figure 17(b) the wetter inland patches in Suriname and Guyana that the other three sets show are not visible for ERA5. In Figure 17(a) CRU shows a spatial difference with ERA5, CHIRPS and GPCC along the border of Guyana and Brazil. CRU does not present the drier patch in that area.

Comparing both Spearman rank correlation and bias between every station and their corresponding GridPrecip grid values, CRU and GPCC show the best scores (correlation close to 1 and bias close to zero) over all stations. ERA5 shows the lowest correlation values of the GridPrecip. Also shown in Figure 17 is the Spearman correlation between certain station observations and the corresponding gridded value precipitation. The GPCP set scores relatively high for the large grid size. CRU, CHIRPS and GPCC score a correlation of at least 0.8 on all of the stations. In Figure 18 the bias between certain station observations and the corresponding gridded value precipitation is shown. CRU and GPCC show the lowest bias values (close to zero), the bias values for ERA5, CHIRPS and GPCP are higher. ERA5 shows a positive bias for almost all stations, meaning drier conditions than for the station observations. GPCP shows a dry bias in Suriname and French-Guiana and a wet bias in Guyana. The bias for CHIRPS does not show a spatial pattern, both negative and positive bias are seen in Figure 18(c).

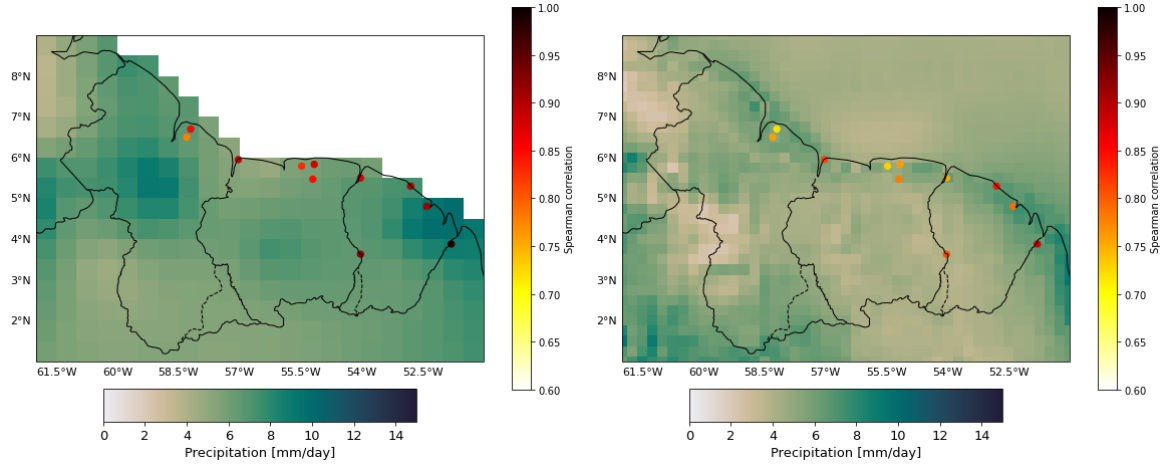


(a) CRU

(b) ERA5

(c) CHIRPS

(d) GPCC

(e) GPCP

**Figure 17:** Spatial distribution of the multi-year annual mean precipitation rates over the period 1981-2000 of (a) CRU (b) ERA5 (c) CHIRPS (d) GPCC (e) GPCP. Including point to grid Spearman rank correlation values between monthly mean station data and GridPrecip.

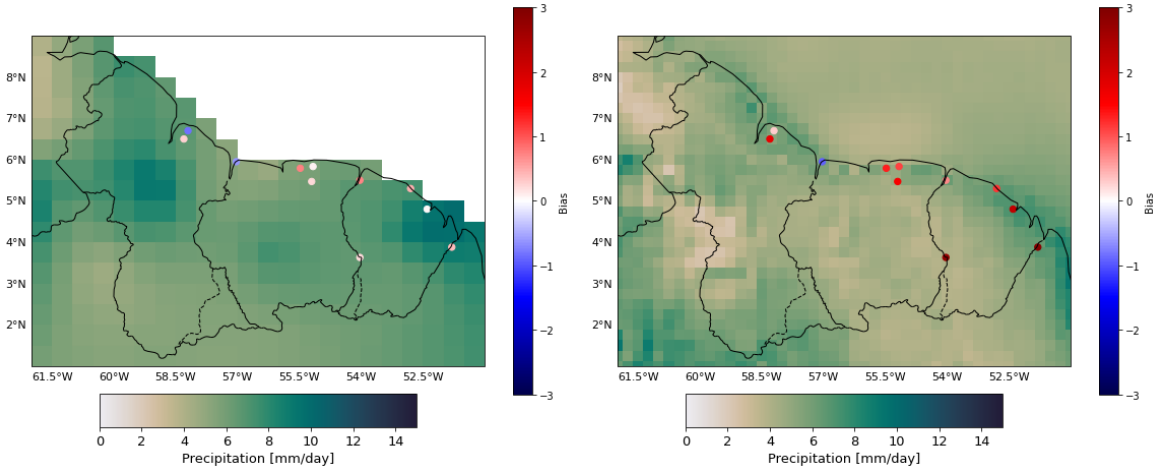


(a) CRU




(b) ERA5

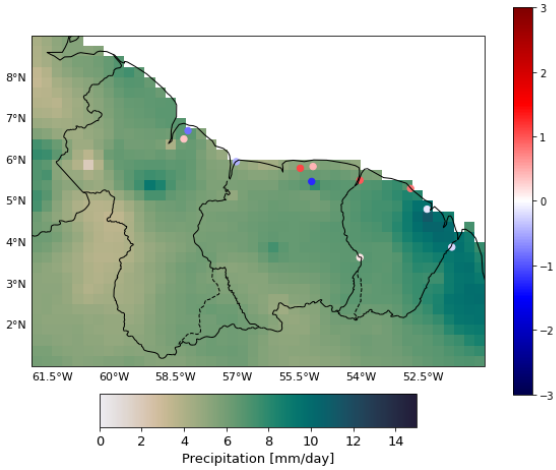


(c) CHIRPS

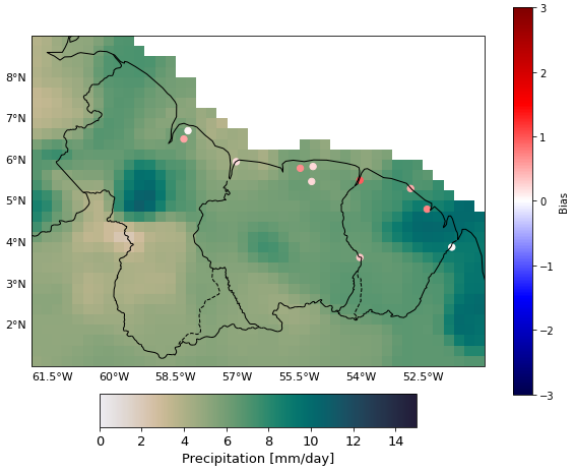


(d) GPCC

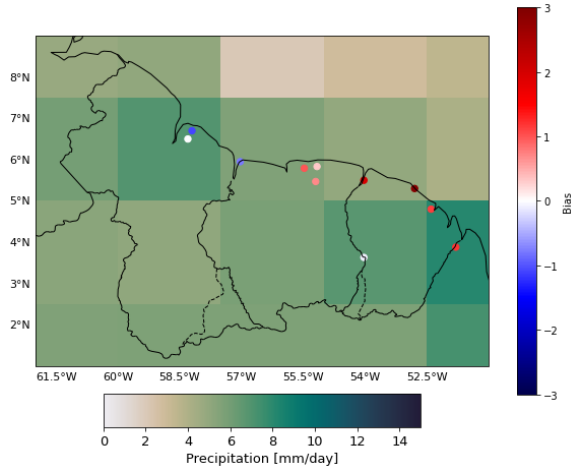


(e) GPCP

**Figure 18:** Spatial distribution of the multi-year annual mean precipitation rates over the period 1981-2000 of (a) CRU (b) ERA5 (c) CHIRPS (d) GPCC (e) GPCP. Including point to grid bias values between station data and GridPrecip.

### Accuracy of daily precipitation

The GPCC and ERA5 dataset do also consist of daily values of precipitation. These daily sets were compared to the stations; Cultuurtuin, Nickerie and Zanderij. The results of the statistics are presented in Table 8. Both the Spearman rank correlation and RMSE show larger differences between the daily gridded sets and station data than the monthly sets. The daily fluctuations of precipitation are not well captured by the GridPrecip in comparison to the monthly fluctuations.

**Table 8:** Average statistics between the GridPrecip sets and observations over the 1981-2000 period consisting daily precipitation data.

| Dataset | Spearman | Spearman anomalies | RMSE (mm/d) | Bias (mm/d) |
|---|---|---|---|---|
| ERA5 | 0.46 | 0.41 | 10.8 | 0.98 |
| GPCC | 0.30 | 0.24 | 13.7 | 0.39 |

### 5.1.2 Comparison between southern and northern parts of Suriname 1976-1986

Since most stations used in the analysis over the period 1981-2000 are located in the coastal areas a different comparison was made to see whether the GridPrecip also display the precipitation well more inland. The data for stations inland is sparse, but the period 1976-1986 gives a data set of 10 years for two inland stations that we can compare directly to CRU, GPCC and ERA5. CHIRPS and GPCP do not have data before the year 1981. The southern, inland region is defined by 4°N-2°N, 58°W-54°W, where the elevation is from 100m to 1000m above sea level. The northern, coastal region is defined by 6°N-4°N, 58°W-54°W, where the elevation remains mainly between 0-100m.

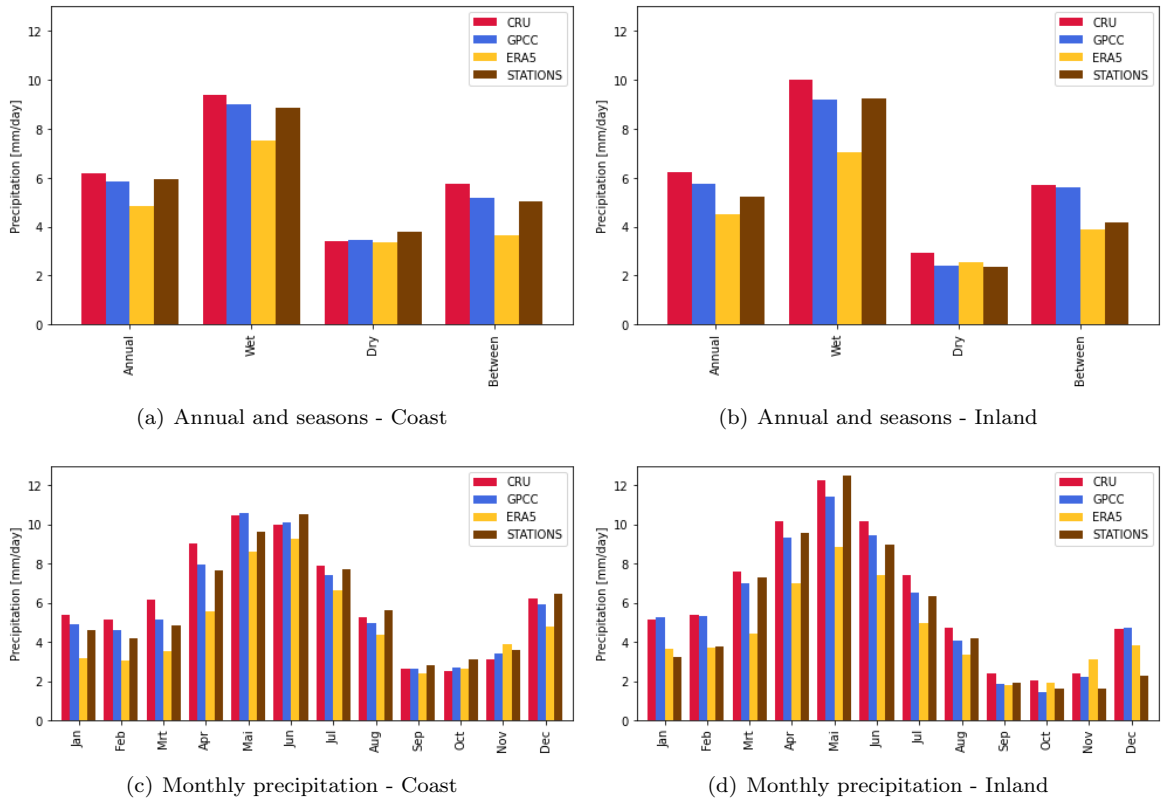


(a) Annual and seasons - Coast

(b) Annual and seasons - Inland

(c) Monthly precipitation - Coast

(d) Monthly precipitation - Inland

**Figure 19:** Precipitation of the coastal (northern) area compared to the inland (southern) area of Suriname for the GridPrecip values (CRU, ERA5, GPCC). For the period 1976-1986. Stations included for the coast comparison are Zanderij, Nickerie, Cultuurtuin and Groningen. Stations included for the inland comparison are Sipaliwini and Kwamalasoemoetoe.

For the coastal area the amount of precipitation measured at the stations lies in between the amount in CRU and GPCC for all seasons except for the dry season. In the dry season all gridded sets underestimate the coastal precipitation. On a monthly basis ERA5 has the largest difference with the stations precipitation. GPCC and CRU overestimate in January, February, March April and May and underestimate in June, July, August, September, October, November and December.

The comparison for the inner land of Suriname shows more difference between the gridded sets and station data. On an annual basis the station precipitation is around the average of the gridded sets. For the wet season GPCC and CRU show values closest to the observations. ERA5 largely underestimates precipitation in the wet season, however for the dry and in-between season ERA5 shows values closest to the observations. On a monthly basis all gridded sets overestimate in the months November, December, January and February. In the months March, April, June, July, August CRU and GPCC are relatively close to the station precipitation. In the month May all gridded sets underestimate the precipitation, CRU is closest.

### 5.1.3 Extended comparison for CRU and GPCC 1952-2000

Both the monthly GPCC and CRU sets scored high on the statistical measures. These sets are compiled from interpolated gauge data and therefore the question arises whether a point-to-grid comparison results in biased results for these sets. In the GPCC set are almost all stations included in the data, or it was unachievable to relate the station density per grid to which exact station was used. Therefore an extended analysis was done for stations that are not included within the CRU set.

**Table 9:** Statistics for CRU per station for the period 1981-2000.

| | Station | Spearman monthly | Spearman anomalies | RMSE monthly [mm/d] | bias monthly [mm/d] |
|---|---|---|---|---|---|
| Annual | Cayenne Rochambeau | 0.91 | 0.71 | 3.4 | 0.040 |
| | Groningen | 0.83 | 0.68 | 2.3 | 0.73 |
| | Timehri | 0.78 | 0.64 | 2.7 | 0.27 |
| | Kuourou | 0.91 | 0.71 | 3.5 | 0.46 |
| | **Average** | **0.86** | **0.69** | **3.0** | **0.40** |

The statistics for CRU compared to the stations that are not included in the set are listed in Table 9. Compared to the statistics for CRU in Table 7, the Spearman correlation went down by about 10%, the RMSE stayed the same and the bias went up almost 5 times. The change in bias can also be the difference between the bias of one station (Table 9) versus the average bias of multiple stations (Table 7). Taking a look at one of those stations that is not included in the CRU dataset (Groningen) in Figure 20 and 21 it can be seen that the scores do not differ that much over a 50 year time period between CRU, where Groningen precipitation is not included and GPCC, where Groningen precipitation is included.

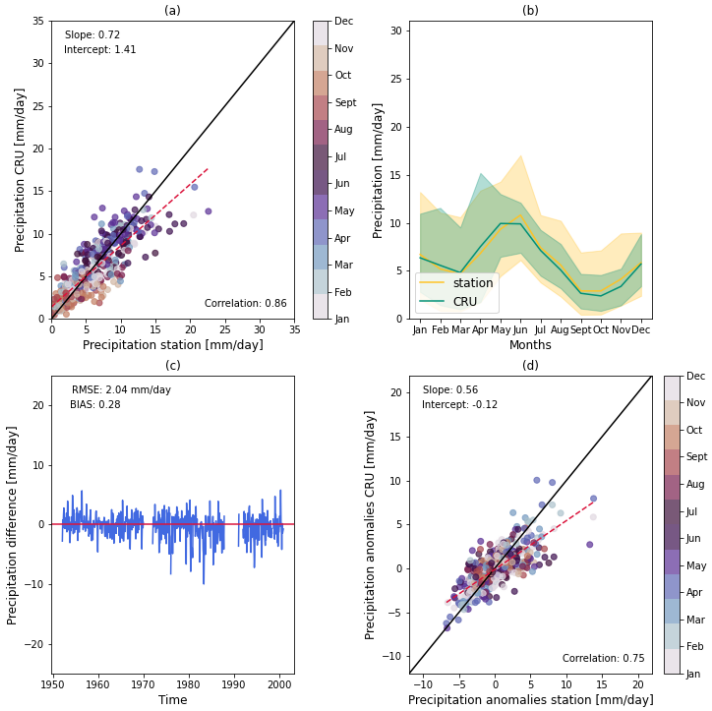


**Figure 20:** Point to grid comparison for the dataset CRU versus station Groningen over the period 1952-2000.

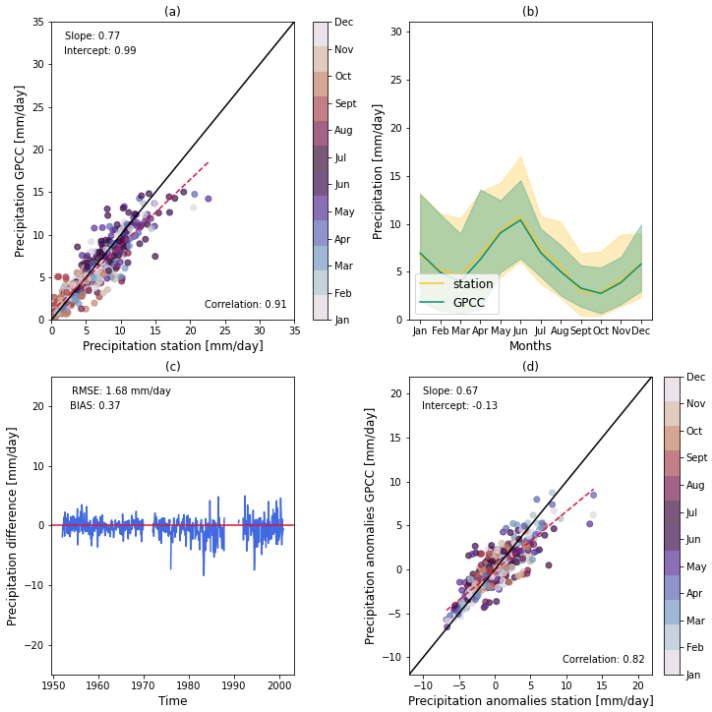


**Figure 21:** Point to grid comparison for the dataset GPCC versus station Groningen over the period 1952-2000.

### 5.1.4 Analysis of 1999-2018

The comparison between stations and GridPrecip for the time period 1999-2018 is very similar to the comparison for the time period of 1981-2000. There are no significant differences in Spearman correlation and RMSE.

**Table 10:** Average statistics between the GridPrecip sets and observations over the 1999-2018 period. Bold score is the best scoring GridPrecip set for that statistic and season.

| | Dataset | Spearman monthly | Spearman anomalies | RMSE monthly [mm/d] | bias monthly [mm/d] |
|---|---|---|---|---|---|
| Annual | CRU | 0.89 | 0.70 | 2.7 | **0.042** |
| | ERA5 | 0.81 | 0.58 | 3.8 | 1.4 |
| | GPCC | **0.95** | **0.87** | **1.6** | 0.38 |
| | GPCP | 0.86 | 0.67 | 3.2 | 0.90 |
| | CHIRPS | 0.90 | 0.740 | 2.4 | -0.31 |
| AMJJ | CRU | 0.83 | 0.70 | 2.4 | **-0.029** |
| | ERA5 | 0.65 | 0.57 | 4.0 | 1.8 |
| | GPCC | **0.96** | **0.94** | **1.3** | 0.30 |
| | GPCP | 0.77 | 0.68 | 3.1 | 0.83 |
| | CHIRPS | 0.82 | 0.75 | 2.6 | -0.64 |
| ASON | CRU | 0.77 | 0.68 | 1.4 | 0.42 |
| | ERA5 | 0.64 | 0.56 | 1.9 | -0.16 |
| | GPCC | **0.89** | **0.82** | **0.94** | **0.078** |
| | GPCP | 0.71 | 0.64 | 1.8 | 0.25 |
| | CHIRPS | 0.84 | 0.75 | 1.2 | -0.14 |
| DJFM | CRU | 0.80 | 0.72 | 3.7 | -0.29 |
| | ERA5 | 0.73 | 0.60 | 4.8 | 2.5 |
| | GPCC | **0.92** | **0.84** | **2.1** | 0.75 |
| | GPCP | 0.77 | 0.67 | 4.1 | 1.6 |
| | CHIRPS | 0.79 | 0.72 | 3.0 | **-0.18** |

## 5.2 Characteristics of historical precipitation data

For the period of 1981-2020 the mean precipitation (averaged over Suriname) in the DJFM season is 5.5 mm/day (median 5.2 mm/day), in the AMJJ season it is 9.0 mm/day (median 9.1 mm/day) and 3.0 mm/day (median 2.9 mm/day) in the ASON season. The seasonal averages per year for Suriname can be viewed in Figure 22. From the vertical lines showing the spread per season, it can be concluded that the AMJJ season has the largest sub seasonal spread in precipitation.

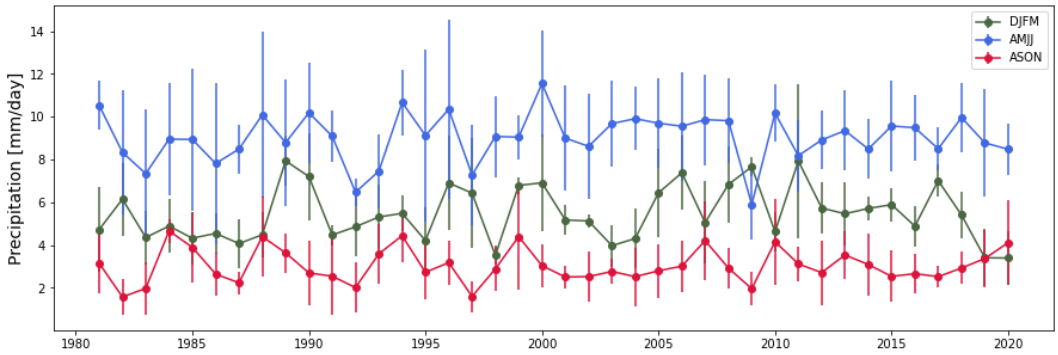


**Figure 22:** Time series of the mean precipitation over Suriname for every season per year: December-January-February-March (DJFM) in green, April-May-June-Juli (AMJJ) in blue, and August-September-October-November (ASON) in red. Including the standard deviation of each season displayed with vertical lines. Data from the Global Precipitation Climatology Centre (GPCC).

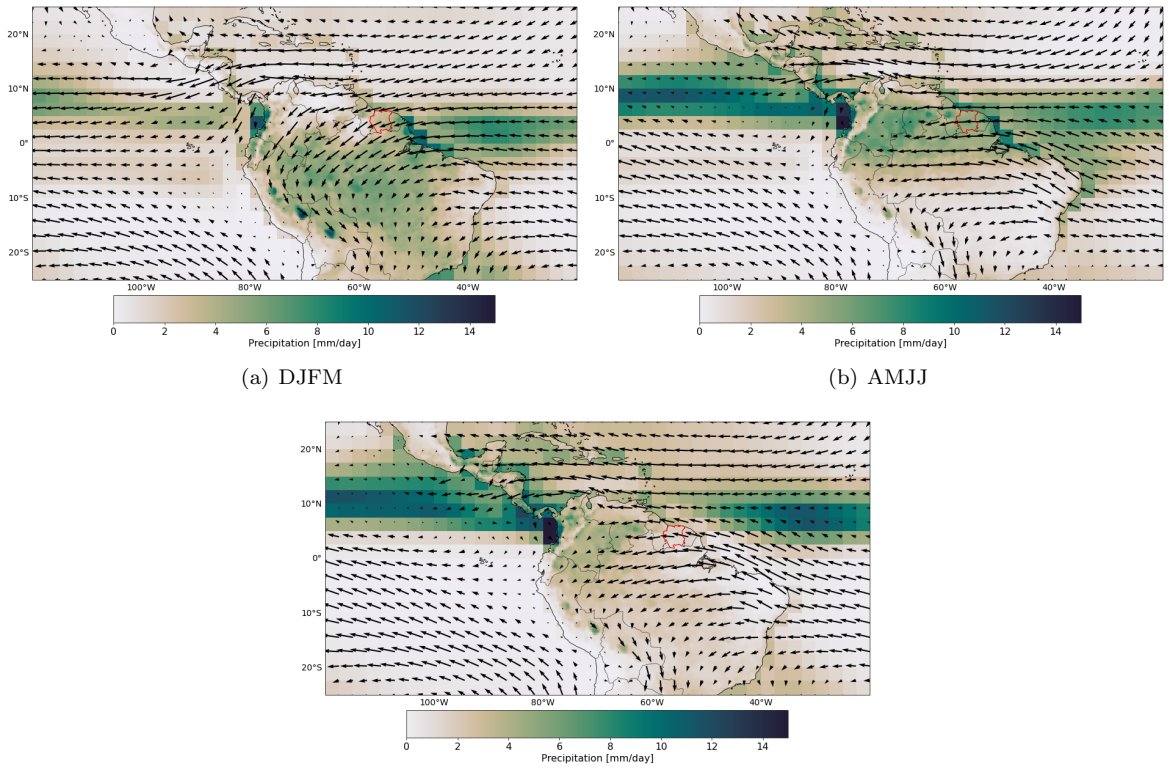


(a) DJFM

(b) AMJJ

(c) ASON

**Figure 23:** Spatial pattern of precipitation climatology (GPCP over ocean and GPCC over land) and 850hPa wind (ERA5) for the period 1981-2020. (a) December-January-February-March (DJFM); (b) April-May-June-July (AMJJ); (c) August-September-October-November (ASON). The country area of Suriname is outlined with red.

In Figure 23 the seasonal pattern of precipitation and the main seasonal wind direction and strength are displayed at 850hPa. In the DJFM season the band of strongest precipitation, corresponding to the ITCZ lies on the south of Suriname. In the AMJJ season Suriname is located in the middle of the ITCZ, and in the ASON season the ITCZ lies above Suriname.

The wind that flows towards Suriname is coming from the North-East and East in the DJFM season, in the AMJJ season it is also coming from the North-East, but deflects towards the East just before reaching Suriname. In the ASON season the wind is coming from the South-East.

**Wet and dry composites**

Since the interest of this study lies in the predictability of precipitation anomalies, whether a season will be drier or wetter than the mean, the precipitation characteristics of the composite years are of interest. The driest years of all three seasons are compared to the wettest years of all three season for the period 1981-2020, based upon the SAI-index and listed in Table 11.

**Table 11:** Years within the period 1981-2022 that exceed 1STD (above) and 0.5STD (below) for all three seasons (DJFM, AMJJ and ASON) and on an annual time scale.

| | **Season** | **wet** | N | **dry** | N |
|---|---|---|---|---|---|
| 1 STD | Annual | 1989, 1990, 1996, 2000, 2005 | 5 | 1983, 1986, 1987, 1992, 2003, 2009 | 6 |
| | DJFM | 1989, 1990, 2000, 2006, 2008, 2009, 2011, 2017 | 8 | 1995, 1998, 2003, 2019, 2020 | 5 |
| | AMJJ | 1981, 1990, 1996, 2000, 2007, 2018 | 6 | 1983, 1986, 1992, 1997, 2009 | 5 |
| | ASON | 1984, 1985, 1988, 1994, 1999, 2007, 2010, 2020 | 8 | 1982, 1983, 1992, 1997, 2009 | 5 |
| 0,5 STD | Annual | 1984, 1989, 1990, 1994, 1996, 2000, 2005, 2007, 2008, 2011, 2013 | 11 | 1982, 1983, 1985, 1986, 1987, 1991, 1992, 1995, 1997, 1998, 2001, 2003, 2009, 2014, 2019, 2020 | 16 |
| | DJFM | 1989, 1990, 1996, 1997, 1999, 2000, 2005, 2006, 2008, 2009, 2011, 2017 | 12 | 1980, 1981, 1983, 1984, 1985, 1986, 1987, 1988, 1991, 1995, 1998, 2001, 2003, 2004, 2010, 2016, 2019, 2020 | 18 |
| | AMJJ | 1981, 1990, 1994, 1996, 2000, 2004, 2005, 2007, 2010, 2018 | 10 | 1982, 1983, 1986, 1992, 1993, 1997, 2001, 2009, 2011, 2014, 2017 | 11 |
| | ASON | 1984, 1985, 1988, 1989, 1993, 1994, 1999, 2007, 2010, 2013, 2020 | 11 | 1982, 1983, 1986, 1987, 1992, 1997, 2001, 2002, 2004, 2009, 2012, 2015, 2017 | 13 |

For temporal patterns of the composite precipitation, the climatology plots of the different composites are displayed in Figure 24. Here it becomes apparent that the Annual, AMJJ and ASON wet and dry composites show differences during the whole year. The DJFM composites are distinctively only different for the actual DJFM season. Another thing to notice is the fact that the composite of a wetter ASON season is corresponding to a drier DJFM season and vice versa. A wetter AMJJ season composite corresponds in general to a wetter overall year. For both the AMJJ and ASON seasons the timing of the peak of the wet season is different for the wet and dry composites. The wet composites peaks earlier than the dry composite for the AMJJ season composites and the wet composite peaks later than the dry composite for the ASON season composites.

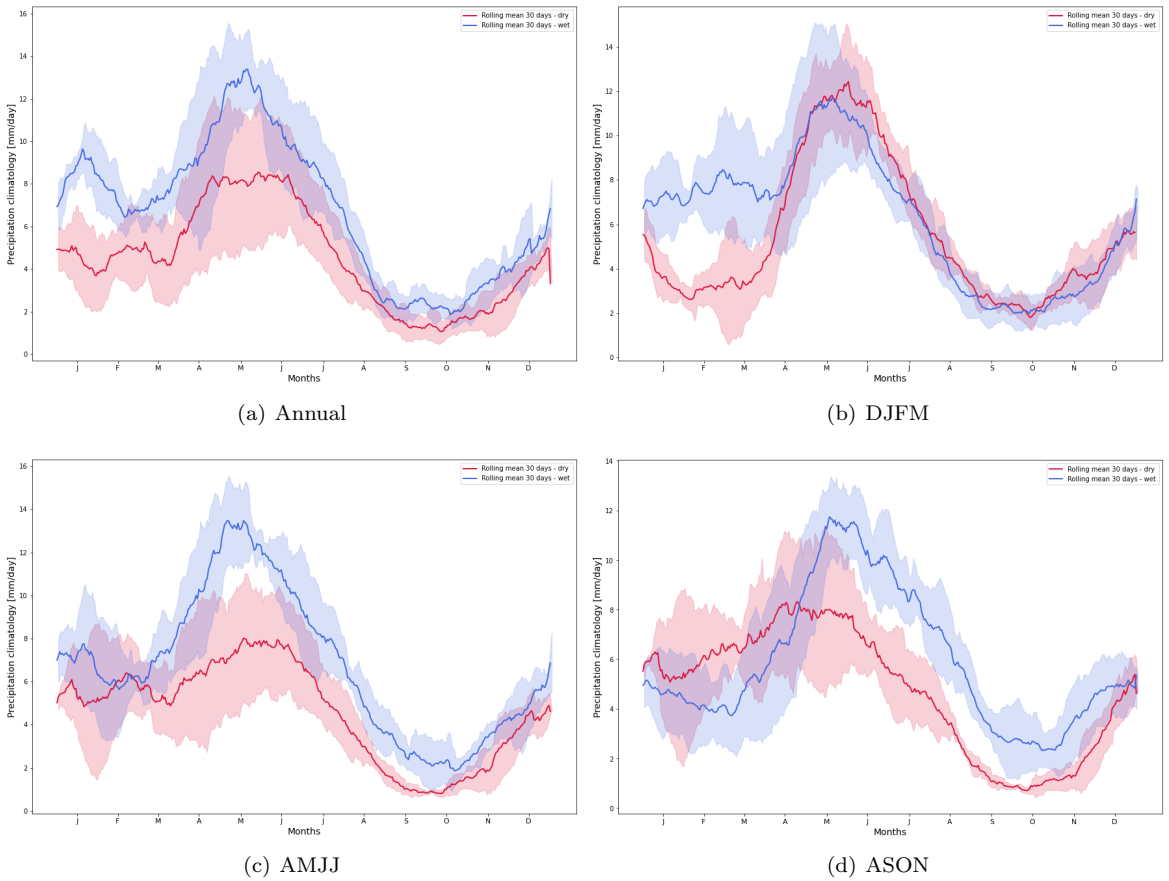


(a) Annual (b) DJFM

(c) AMJJ (d) ASON

**Figure 24:** Wet and dry composites of the GPCC precipitation (the years included in these composites can be found in Table 11). The bands show precipitation within 1 standard deviation. (a) Annual; (b) December-January-February-March; (c) April-May-June-July; (d) August-September-October-November.

When looking at the spatial pattern of the difference between the wet and dry composites in Figure 25, there is a difference visible over the Pacific and the Atlantic for all seasons. For the dry composites the Atlantic experiences less precipitation and the Pacific experiences more precipitation in comparison to the wet composites, and vice versa. This pattern is strongest in the AMJJ and ASON season. Overall Suriname follows the same pattern as the Atlantic. The strongest differences are visible in the DJFM season for the coast in front of the Guianas and French-Guiana itself (more than 4 mm/day) and in the AMJJ season over the Guiana shield (3-4 mm/day). The difference over the Pacific is strongest (more than 4 mm/day) for the ASON season.

Easterly winds dominate the wind pattern over Suriname all year. For the DJFM and AMJJ season a small dipole is visible over both the Pacific and Atlantic ocean, which could indicate a shift of the ITCZ. This encompasses that over the Atlantic the ITCZ moves north in the AMJJ in the dry composite compared to the wet composite and in the DJFM season the ITCZ moves south in the dry composite compared to the wet composite. In the DJFM season the general position of the ITCZ is on the Southern end of Suriname, a further movement south would therefore indeed enhance drought in Suriname. In the AMJJ season the ITCZ moves from south to north over Suriname, a further movement north of the ITCZ could mean a shorter traverse of the ITCZ over Suriname and therefore drier conditions.

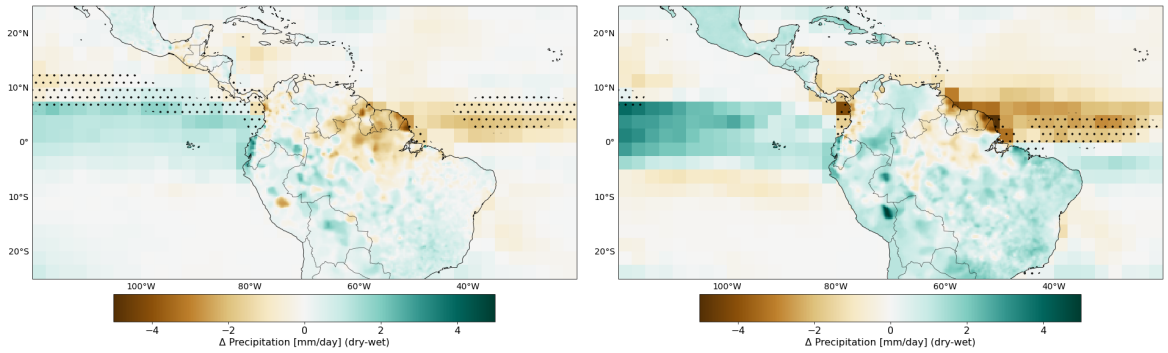


(a) Annual




(b) DJFM

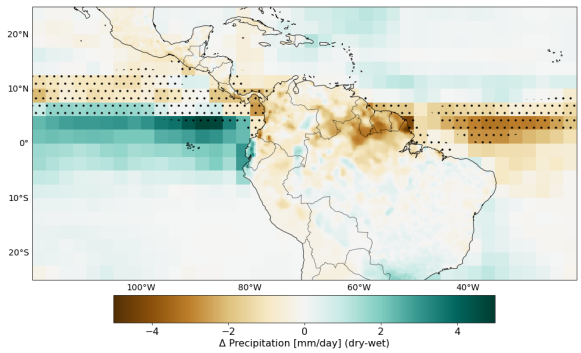


(c) AMJJ

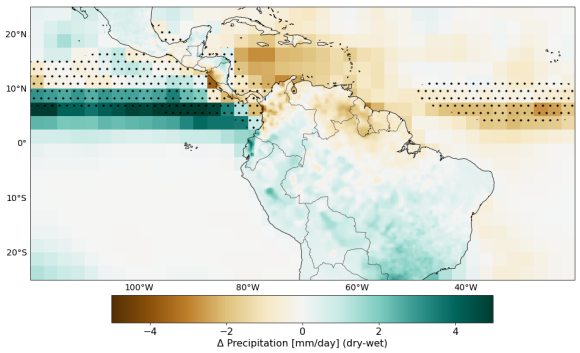


(d) ASON

**Figure 25:** Spatial wet minus dry composites of the GPCC precipitation patterns (years included in these composites can be found in Table 11). The dotted areas show the climatology (1981-2020) of the ITCZ position, defined by precipitation values higher than 6 mm/day. (a) Annual; (b) December-January-February-March (DJFM); (c) April-May-June-July (AMJJ); (d) August-September-October-November (ASON).

## 5.3 Sea surface temperature correlation

To investigate the relationship between sea surface temperature anomalies and precipitation anomalies in Suriname, maps of the spatial pattern of Spearman rank correlation between the time series of SSTA and the anomalies to the average Suriname precipitation values were made. The correlations of three different seasons are presented with zero, one month and two months lag between the precipitation anomalies and the SSTA's in Figure 26.

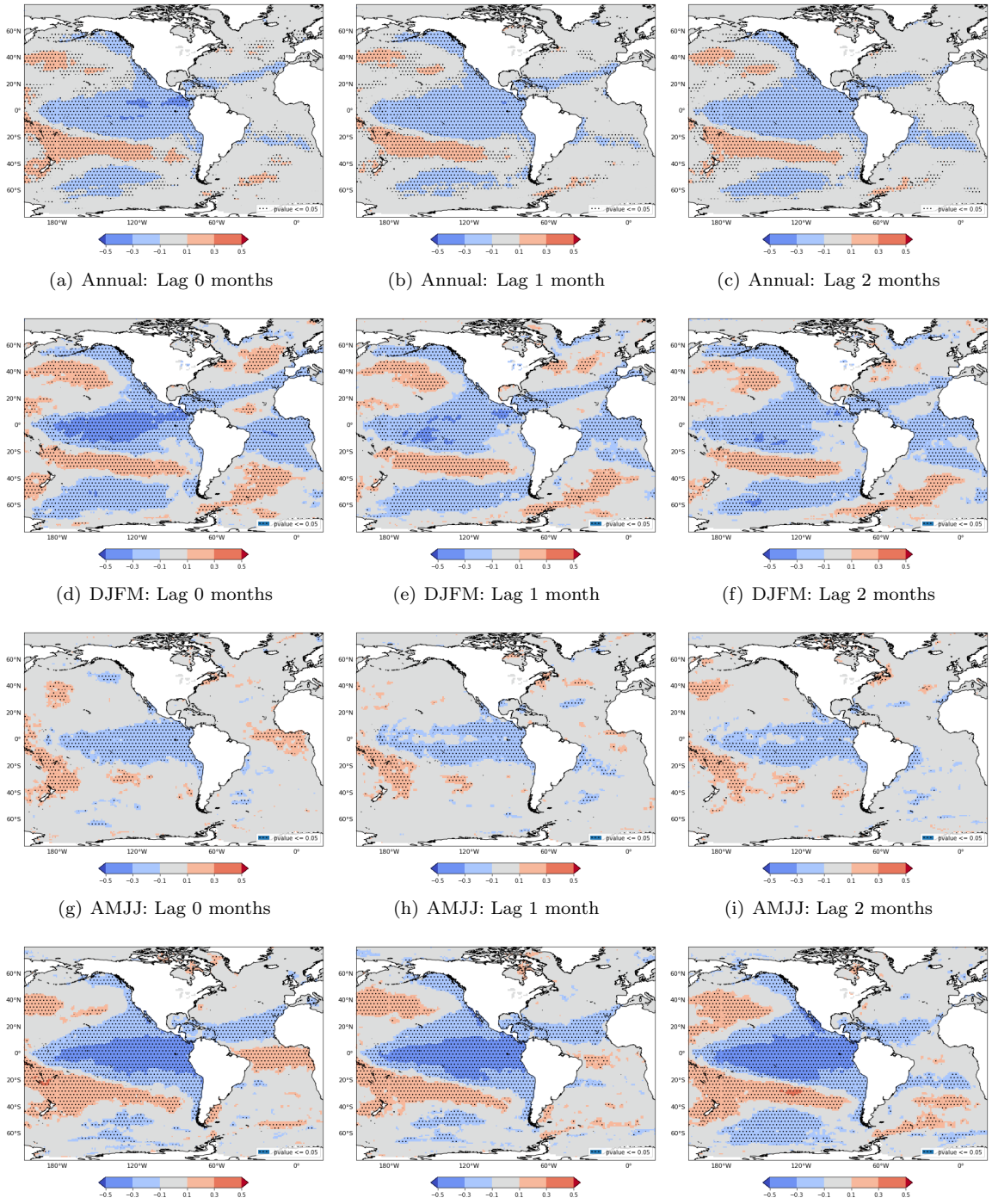

(a) Annual: Lag 0 months (b) Annual: Lag 1 month (c) Annual: Lag 2 months

(d) DJFM: Lag 0 months (e) DJFM: Lag 1 month (f) DJFM: Lag 2 months

(g) AMJJ: Lag 0 months (h) AMJJ: Lag 1 month (i) AMJJ: Lag 2 months

(j) ASON: Lag 0 months (k) ASON: Lag 1 month (l) ASON: Lag 2 months

**Figure 26:** The correlations of three different seasons are presented with zero, one month and two months lag between the precipitation anomalies and the SSTA's for the period 1950-2020.

For the correlation of the entire time series of anomalies (Annual) the strongest correlation patterns are seen over the Pacific (Figure 26(a)). Around the equator there is a large area (circa 20°N-20°S) with a negative correlation between 0.1 and 0.3. Within this area there are two patches that show a stronger negative correlation between 0.3 and 0.5, these are located at 5-10°N and 120°W and 90°W. A dipole pattern is shown further over the Pacific with a positive correlation around 30°S and another negative correlation at around 60°S. Also along the West Coast of the North American continent a negative correlation is visible. Over the Atlantic there are no large areas of correlation. Only two bands of negative correlation can be found around 20°N and 20°S. When a lag of 1 or 2 months is added, the spatial pattern of correlation remains the same as with zero lag. The correlation strength does decrease with increasing lag time.

For the DJFM season (Figure 26(d)) a similar spatial correlation pattern over the Pacific is visible as for the annual time series. The strength of the negative correlation visible over the Pacific around the location of the equator is stronger for this season than for the annual time series. The negative correlation at the Pacific around the equator is strongest for a lag of 0 months and corresponds to the location of the ENSO indices; Nino3, Nino4 and Nino3.4. The index Nino1+2 lies more towards the south (0° -10°S, 90°-80°W) than the stronger patch of correlation in this figure (5°-10°N, 85°-95°W ). At the Atlantic a different pattern is visible compared to the annual time series. There is a large area of negative correlation between 0° and 30-40°S. A small dipole pattern of correlation can be found north of this area, with a positive correlation at around 10°N and another negative correlation at circa 20°N. At both 40-60°N as 40-60°S a positive correlation over the Atlantic is visible. With a lag of 1 or 2 months the spatial pattern of correlation stays similar for both the Pacific and Atlantic, however the strength of the correlation does decrease with increasing lag time. The only exception is the band of negative correlation over the Atlantic at around 20°N.

The AMJJ season shows the least correlation of the three seasons. The same negative correlation patch at the Pacific corresponding to the ENSO indices can be found, although it is smaller than in the other seasons. Over the Atlantic almost no significant correlation can be seen. An exception is a positive correlation around the equator at 20°W to 10°E, which is an indication of the Atlantic Niño. This pattern vanishes when a lag is introduced. Something that does occur in both the DJFM and AMJJ season is a patch of positive correlation with the SSTAs around 40°N, 60°W, along the east coast of North America. The AMJJ season correlation decreases with increasing lag time.

The ASON season (Figure 26(j)) shows a similar correlation pattern over the Pacific as the annual time series. The area around the equator shows a clear negative correlation (0.3-0.5). The area around 60°S shows a positive correlation (0.1-0.3), which becomes larger in the center for a lag of two months. Over the Atlantic a clear dipole is visible, with a positive correlation beneath the equator and a negative correlation above the equator. The dipole over the Atlantic is strongest with lag 0 and becomes smaller when a greater lag was created. Where overall the correlation with zero lag time is the strongest, this is not the case for the ASON season. Here the strongest correlation is found with a lag of 3 and 5 months. This pattern can be seen in Figure 27. The strongest positive correlation is visible around 30°S, 120°W. The strongest negative correlation is within the area 0-20°S, 180-100°W.

Overall the spatial pattern of correlation over the Pacific is similar for all seasons and is therefore also clearly visible in the annual correlations. The correlation over the Pacific does differ in strength per season. The spatial pattern of correlation over the Atlantic is different for every season and therefore vanishes in the annual correlation. All correlations, except for the band over the Atlantic at 20°N in the DJFM season and the Pacific correlation in the ASON, decrease with increasing lag time. The strongest correlations found for each season and the corresponding lag time are presented in Table 12.

**Table 12:** Maximum correlation values between SSTA and precipitation anomalies per season.

| Season | max. positive correlation | max. negative correlation |
|---|---|---|
| DJFM | 0.31 (Lag 0) | -0.38 (Lag 0,1) |
| AMJJ | 0.25 (Lag 2) | -0.26 (Lag 0,1) |
| ASON | 0.38 (Lag 5) | -0.45 (Lag 3) |

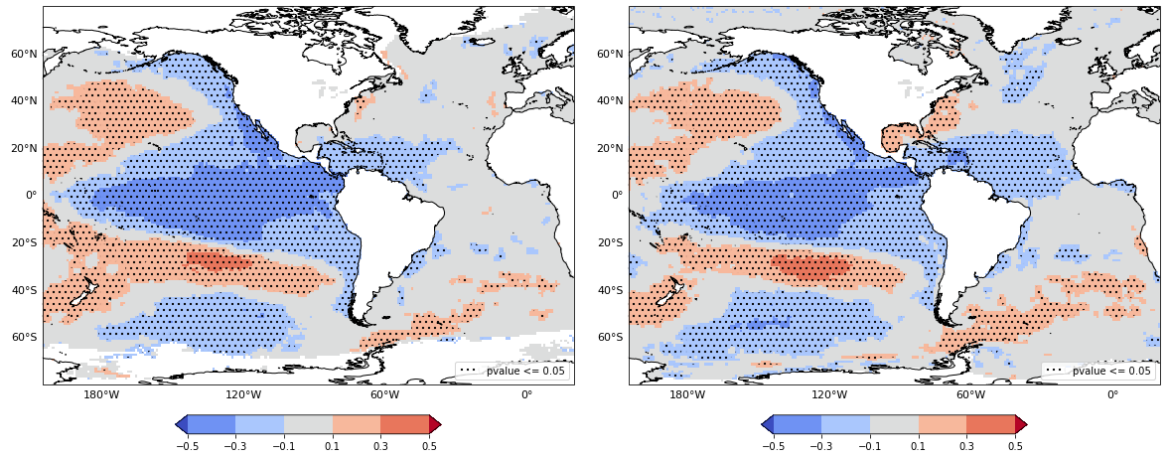


(a) Dry season (ASON) lag 3

(b) Dry season (ASON) lag 5

**Figure 27:** Anomalies of precipitation correlated with anomalies of SST for the period 1950-2020 for the ASON season with a lag of 3 and 5 months

Besides the Spearman correlation a linear regression between SSTAs and Suriname's precipitation anomalies was also applied. In Figure 28 the spatial pattern of a linear least-squares regression between the time series of SSTA and the anomalies to the average Suriname precipitation values are given. The slope of the linear regressions, in mm/day difference per 1 degree °C SSTA change, of three different seasons are presented with zero, one month and two months lag between the precipitation anomalies and the SSTA's.

In general the spatial patterns of the slope of the linear regression and the correlations for the annual time series complement each other. Around the Pacific equator the areas of highest correlation and regression do differ in location, and around 60°S there are stronger regression patterns than correlation patterns. This can give a distorted picture because the equatorial regions experience larger and more dynamic SST differences than the higher latitudes.

Over the Atlantic the patterns for the slope of the linear regression are more pronounced than for the correlation, which indicates there is indeed a relation between the SSTA's in the Atlantic and precipitation anomalies in Suriname, however it is distorted by outliers and therefore difficult to use for predictions.

The strongest regression pattern can be seen for the DJFM season, indicating that a small perturbation in SST leads to larger precipitation anomalies in the DJFM season than the other seasons. However taken the correlation patterns into account; large variations in precipitation and SST are expected for the DJFM season.

The AMJJ season shows a different pattern for the regression than for the correlation. The negative area at the Pacific from 20°N to 20°S is similar. Around the equator at the Atlantic a positive regression is seen for a lag of 0 months, this area is typically related to the Atlantic Niño (3°S–3°N, 0–20°W). With increasing lag this positive area decreases in regression strength, contrary to the Atlantic on the east coast of South America between 0° and 20°S were a negative regression increases with increasing lag time. The area around 45°S, 90°W at the Pacific shows a strong positive regression for every month of lag that is added.

The ASON regression patterns are less pronounced than the ASON correlation patterns. Even so the spatial pattern is similar. This indicates a strong connection of precipitation to SST patterns for the ASON season.

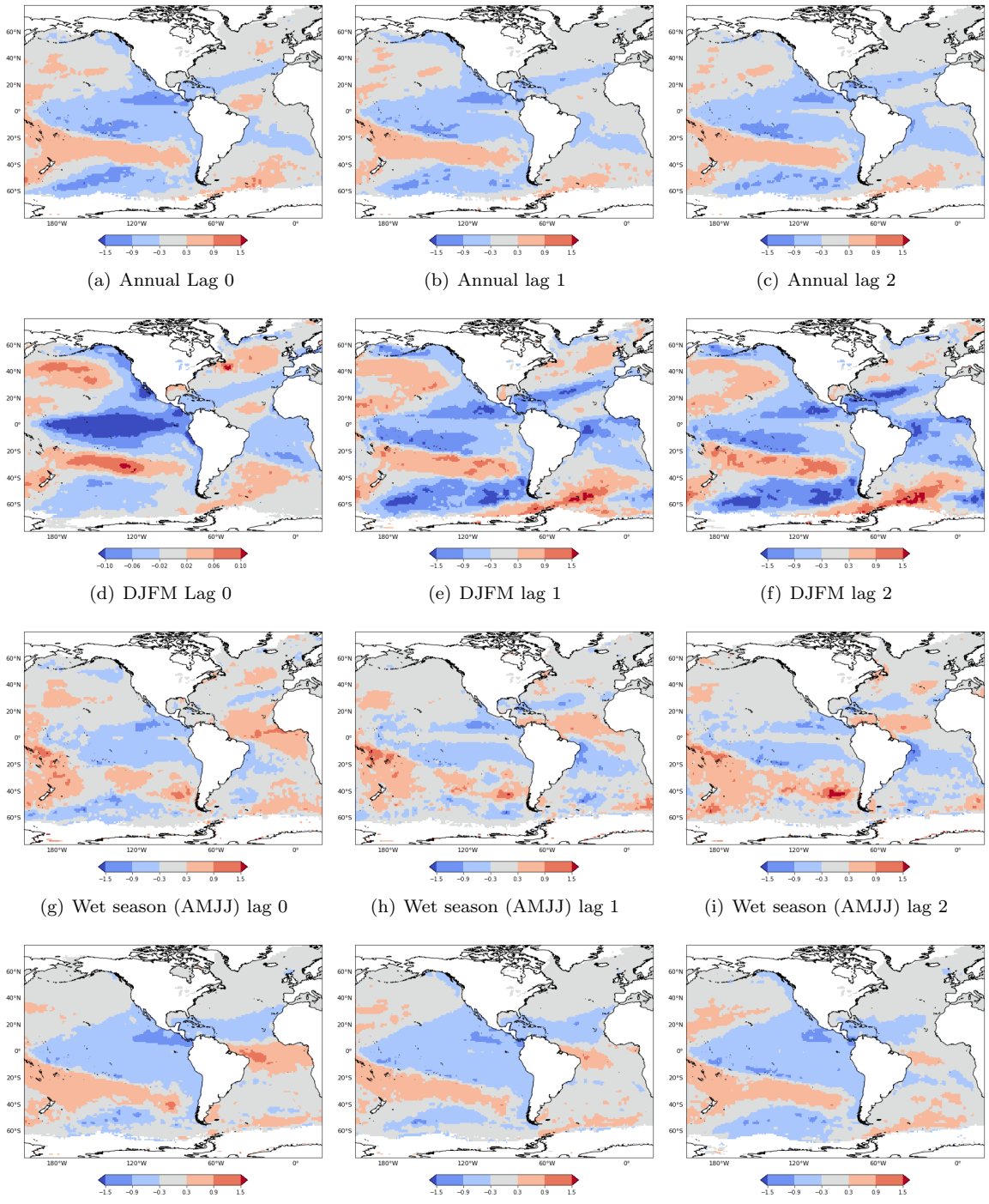

(a) Annual Lag 0 (b) Annual lag 1 (c) Annual lag 2

(d) DJFM Lag 0 (e) DJFM lag 1 (f) DJFM lag 2

(g) Wet season (AMJJ) lag 0 (h) Wet season (AMJJ) lag 1 (i) Wet season (AMJJ) lag 2

(j) Dry season (ASON) lag 0 (k) Dry season (ASON) lag 1 (l) Dry season (ASON) lag 2

**Figure 28:** Slope of the linear regressions (ΔPrecipitation [mm/d] / ΔSST [°C]) for Annual, DJFM, AMJJ and ASON are presented with zero, one month and two months lag between the precipitation anomalies and the SSTA's for the period 1950-2020

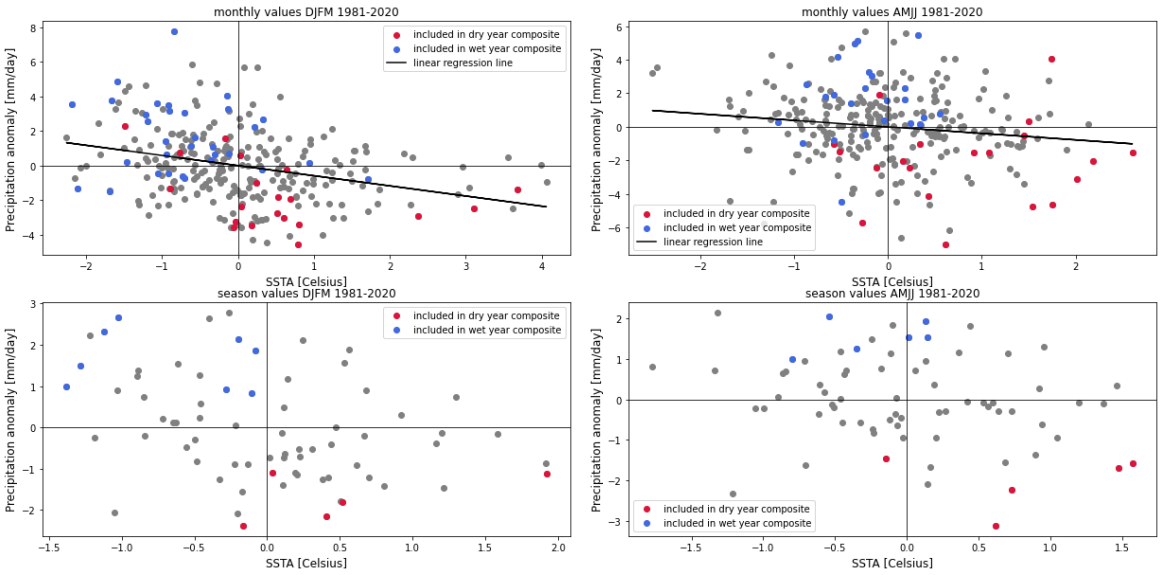


(a) DJFM




(b) AMJJ

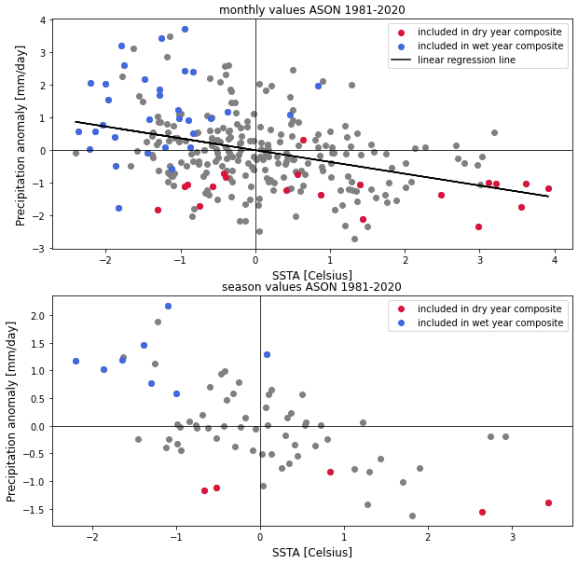


(c) ASON

**Figure 29:** Scatterplot of SSTA versus precipitation anomalies at the location of a self-defined index: Pacific index 1 [2S-2N,122W-118W]. Red colors indicate the monthly values (above) or season values (below) of years that are included in the dry composite. Blue colors indicate the monthly values (above) or season values (below) of years that are included in the wet composite. (a) DJFM Lag 0 monts (b) AMJJ Lag 0 months (c) ASON Lag 0 months

To compare the correlation of Suriname precipitation anomalies with pre-existing work, the strongest correlation, and its corresponding lag time, for well defined indices of certain teleconnection patterns are presented in Table 13. Most indices show the strongest correlation with Suriname precipitation anomalies for a lag of 0 months. The correlations of indices in comparison to the correlations of Nurmohamed et al. (2007) can be found in Appendix C. The correlations averaged over an index area are not that strong. The highest correlations are between 0.3 and 0.4. The ASON season is the only season that shows evidence of skill in the months prior to an precipitation event.

Figure ?? shows scatterplots for all three season at the location of the Pacific index 1, a self-defined index over the equatorial Pacific that is smaller than pre-existing indices to avoid the large averages

taken. The wet composites fall mainly in the left upper quadrant. The dry composites show more spread and therefore no clear connection to ENSO.

**Table 13:** Spearman correlation between predefined indices and precipitation anomalies. Correlations that are significant with $p \leq 0.05$ ($p \leq 0.01$) are indicated with an * (**).

| **Index** | **Correlation (Annual)** | **Correlation (DJFM)** | **Correlation (AMJJ)** | **Correlation (ASON)** |
|---|---|---|---|---|
| Nino12 | $r_{lag0}$ = -0.26** | $r_{lag0}$ = -0.20** | $r_{lag0}$ = -0.21** | $r_{lag0}$ = -0.41** |
| Nino3 | $r_{lag0}$ = -0.30** | $r_{lag0}$ = -0.35** | $r_{lag0}$ = -0.18** | $r_{lag0,3}$ = -0.39** |
| Nino3.4 | $r_{lag0}$ = -0.29** | $r_{lag0}$ = -0.35** | $r_{lag0}$ = -0.16** | $r_{lag3}$ = -0.38** |
| TNA | $r_{lag2,5}$ = -0.079* | $r_{lag2}$ = -0.12* | $r_{lag0}$ = 0.061 | $r_{lag5}$ = -0.19** |
| TSA | $r_{lag2}$ = -0.063 | $r_{lag0}$ = -0.26** | $r_{lag0}$ =0.068 | $r_{lag0}$ = 0.14* |
| Pacific index 1 | $r_{lag0}$ = -0.27** | $r_{lag0}$ = -0.33** | $r_{lag0}$ = -0.15* | $r_{lag3-4}$ = -0.37** |
| Pacific index 2 | $r_{lag3,4}$ = 0.21** | $r_{lag2}$ = 0.23** | $r_{lag4}$ = 0.13* | $r_{lag5}$ = -0.34** |
| Atlantic Nino | - | $r_{lag0}$ = -0.24** | $r_{lag0}$ = 0.13* | $r_{lag5}$ = 0.19** |

## 5.4 Moisture tracking

In this section the results of moisture tracking with WAM2layers are presented per season. Over all the seasons it can be seen that most moisture that precipitates in Suriname originates from the Atlantic ocean. The moisture is transported from the Atlantic ocean towards Suriname with the direction of the trade winds. In general the moisture recycling of Suriname is relatively low indicating that most moisture is originating over the ocean and not over land. On average the recycling ratio ($\rho_c$) of Suriname is 10%. According to Van Der Ent et al. (2010), the global average precipitation recycling ratio ($\rho_c$) is 40%.

### 5.4.1 DJFM season

**Table 14:** Recycling ratios for the composites of the DJFM season.

| Composite | $e_r$[%] | $\rho_r$[%] | $\rho_c$[%] |
|---|---|---|---|
| DJFM Wet | 11.2 | 6.5 | 16.5 |
| DJFM Dry | 2.7 | 2.4 | 4.9 |

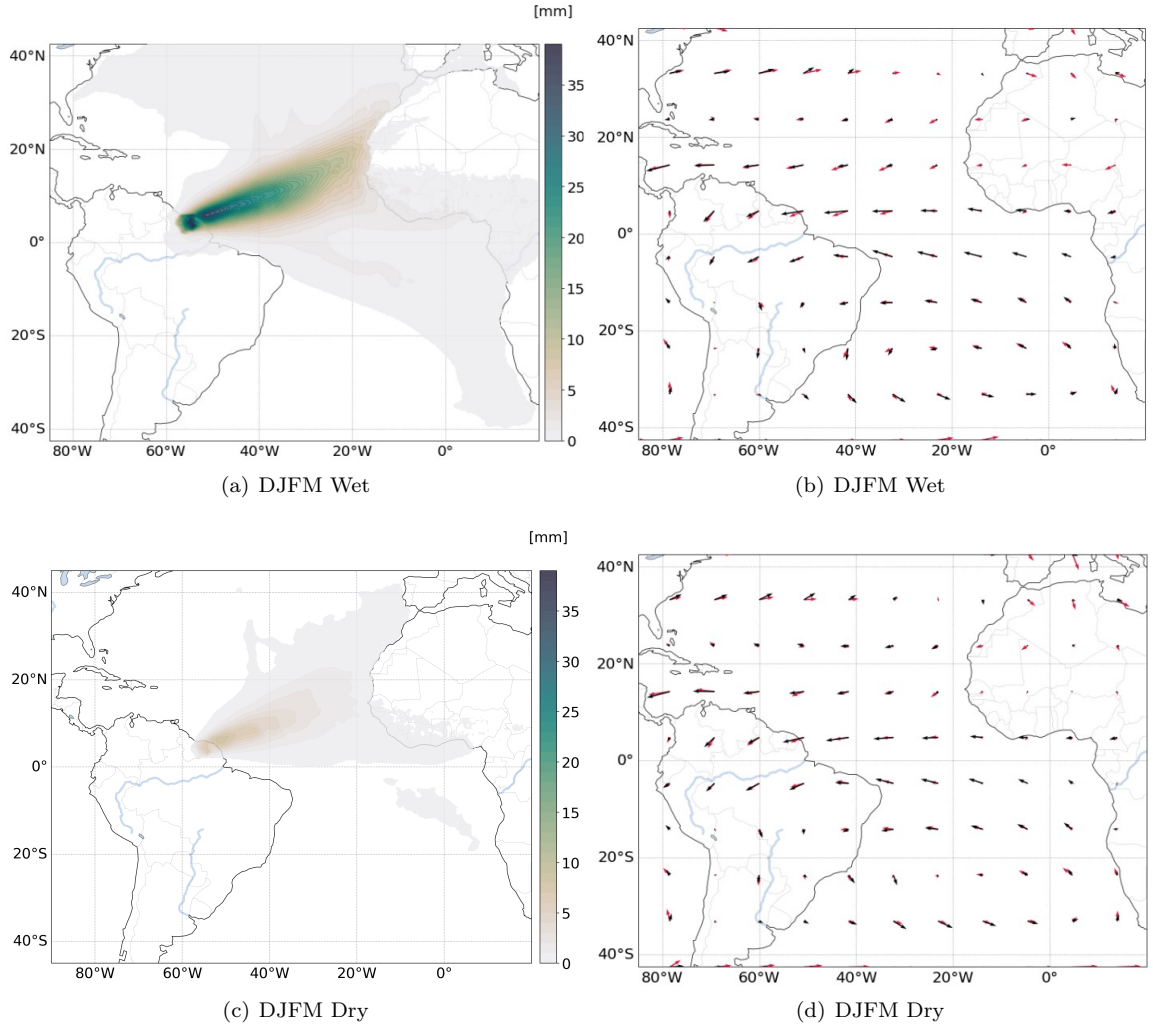


(a) DJFM Wet

(b) DJFM Wet

(c) DJFM Dry

(d) DJFM Dry

**Figure 30:** Evaporation moisture tracking results for the DJFM season for the years 2009,2011,2017 (wet) and 2003,2019,2020 (dry). On the left the amount of tracked evaporation. On the right the moisture transport (black arrows) and the 850hPa wind (red arrows).

The absolute amount of tracked evaporation for the wet DJFM composite is more than 4 times as high as the tracked evaporation for the dry DJFM composite. The path from where the precipitation in Suriname originates is similar for both composites. The evaporation does originate further away from Suriname in the wet composite. The wind and moisture transport direction and size are similar for both composites. The main difference between the wet and dry composites for the DJFM season is the amount of recycling. The continental precipitation recycling rate goes from 5% in the dry composite to 16.5% in the wet composite. Compared to the AMJJ wet composite (Figure 31(a)) that has a higher amount of total precipitation and tracked evaporation, the DJFM wet composite (Figure 30(a))shows much less spread of the evaporation origin area. Resulting in high concentrations following the path of the north easterlies.

### 5.4.2 AMJJ season

**Table 15:** Recycling ratios for the composites of the AMJJ season.

| Composite | $e_r$[%] | $\rho_r$[%] | $\rho_c$[%] |
|---|---|---|---|
| AMJJ Wet | 14.5 | 5.1 | 8.9 |
| AMJJ Dry | 7.6 | 5.3 | 7.7 |

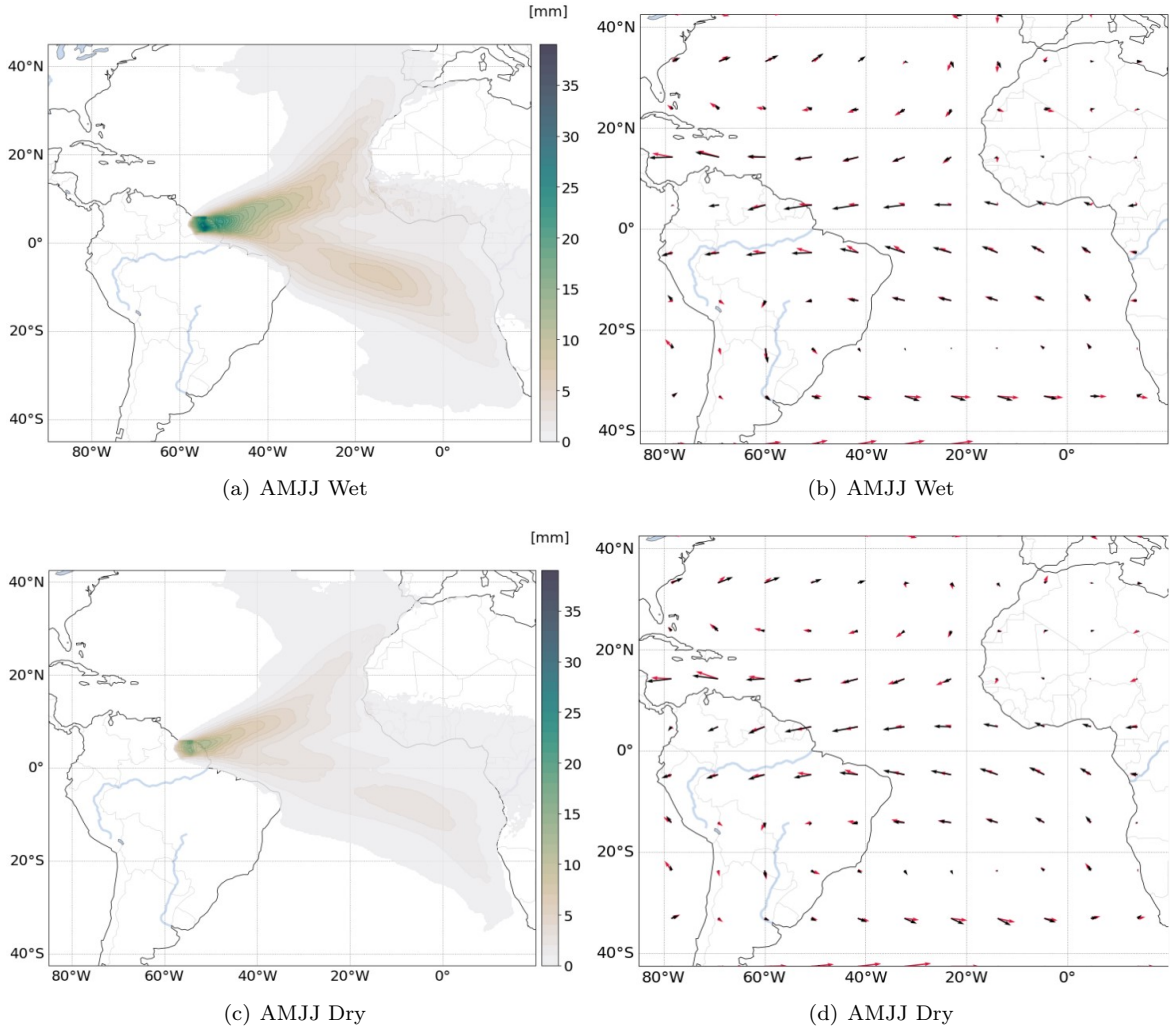


(a) AMJJ Wet

(b) AMJJ Wet

(c) AMJJ Dry

(d) AMJJ Dry

**Figure 31:** Evaporation moisture tracking results for the AMJJ season for the years 20000,2007,2018 (wet) and 1992,1997,2009 (dry). On the left the amount of tracked evaporation. On the right the moisture transport (black arrows) and the 850hPa wind (red arrows).

The precipitation recycling ratios for both AMJJ composites are similar as seen in Table 15, although the evaporation recycling ratio of the wet composite is twice as large as the recycling ratio for the dry composite. The origin of the moisture is similar for both composites. The only change seems to be in the absolute amount of tracked evaporation, due to the higher amount of precipitation in the wet composite.

### 5.4.3 ASON season

**Table 16:** Recycling ratios for the composites of the ASON season.

| Composite | $e_r$[%] | $\rho_r$[%] | $\rho_c$[%] |
|---|---|---|---|
| ASON Wet | 6.3 | 5.5 | 10.4 |
| ASON Dry | 2.1 | 4.1 | 6.7 |

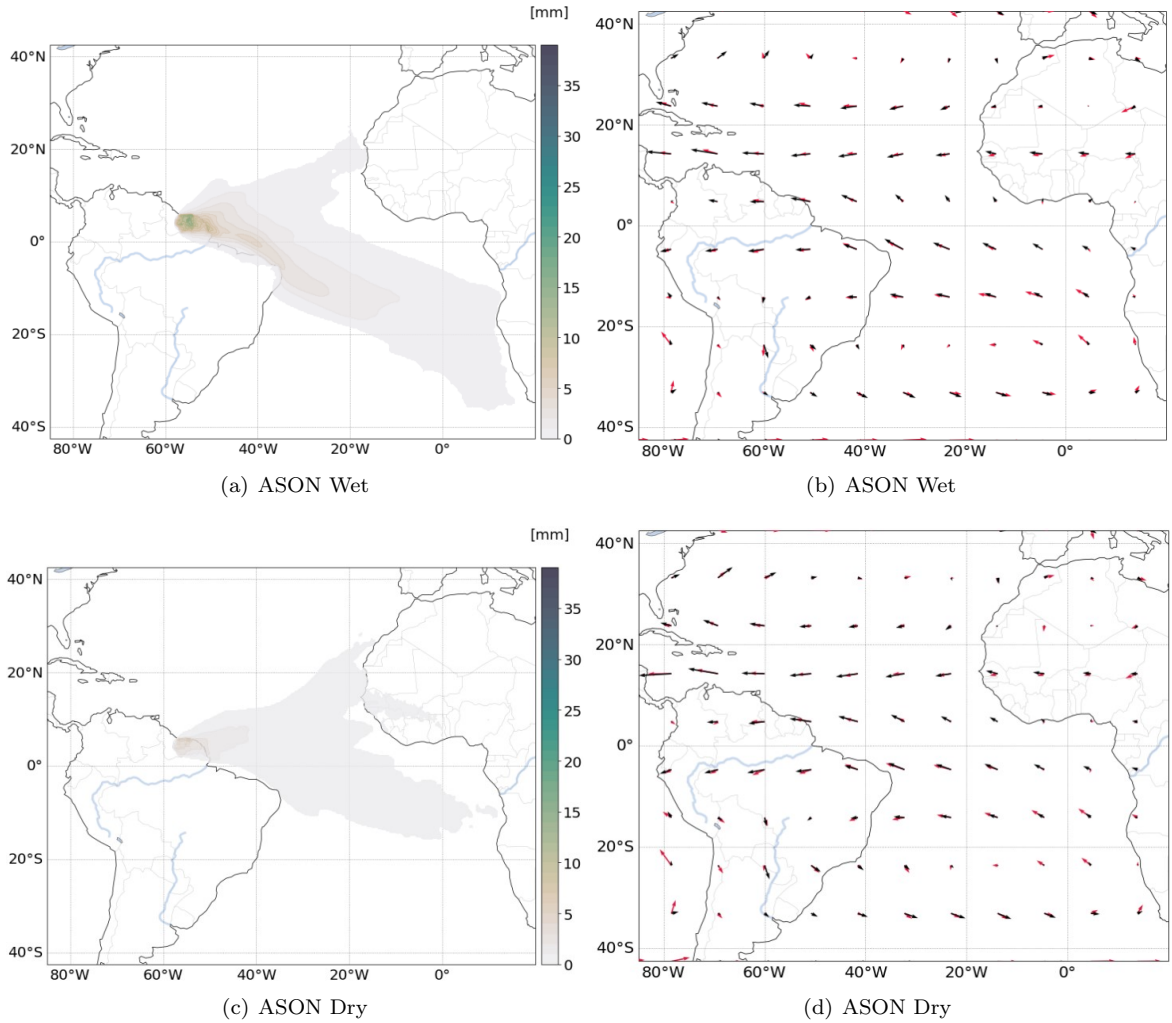


(a) ASON Wet (b) ASON Wet

(c) ASON Dry (d) ASON Dry

**Figure 32:** Evaporation moisture tracking results for the ASON season for the years 2007,2010,2020 (wet) and 1992,1997,2009 (dry). On the left the amount of tracked evaporation. On the right the moisture transport (black arrows) and the 850hPa wind (red arrows).

The absolute difference between the amount of precipitation for the wet and dry composite is not that large, the wet composite has about 1.3 times more precipitation than the dry composite. The recycling ratios of both composites are similar, although the continental recycling ratio of the wet composite

(Figure 32(a)) is 10% larger than the recycling ratio for the dry composite (Figure 32(c)). The origin of the moisture for the wet composite is in comparison to the dry composite more from the southern hemisphere than the northern hemisphere.

# 6 Discussion

In this section, the results of Section 5 are further explored. From the moisture tracking analysis it became clear that almost all precipitation ending up in Suriname originates over the Atlantic ocean ( 90%). The direct link between Atlantic SSTA and precipitation anomalies in Suriname is therefore further explored in Section 6.1. The correlations between SSTA and precipitation anomalies showed a strong correlation with Pacific SSTAs, which is therefore further explored in Section 6.2. Section 6.3 discusses further teleconntections that influence precipitation in Suriname and section 6.4 concludes with some recommendations for future studies.

## 6.1 Combining Atlantic sea surface temperature correlations and moisture tracking towards the drivers of precipitation anomalies

In the DJFM season the location of the band of evaporation over the Atlantic does not correspond to a band of correlation with SSTA, but is wrapped in between two bands of negative correlation. In Figure 33(a) the difference in SST between the wet and dry composites are presented (dry-wet). Here it can be seen that the band of origin evaporation shows a difference of circa 1 degree between the wet and dry composites. Consistent with the fact that warmer SST cause more evaporation to occur and therefore also more precipitation. This difference in SST is part of a small dipole visible in the Atlantic ocean with colder waters above the equator and warmer waters below the equator for the wet composites. This relates to the findings of Cabos et al. (2019) about the Tropical Atlantic Variability (TAV). For a so-called negative AMM mode of the TAV the ITCZ shifts further south, which would place the ITCZ below Suriname and therefore relates to drier conditions over Suriname. This pattern was also visible in Figure 25. This dipole pattern is visible in the correlation with SSTA, where a negative correlation is shown from 0° to 20°S over the Atlantic, meaning that colder (warmer) SSTs below the equator cause more (less) precipitation over Suriname. This is again indicating a positive (negative) AMM mode. An even more pronounced pattern is the dipole over the North Atlantic with negative correlation around 20°N. This pattern becomes more apparent with increasing lag and therefore suggests some skill. Both these patches of negative correlation correspond to a change in wind speed and direction at 10m between the wet and dry composites (Figure 33(a)).

For the AMJJ season there was no significant correlation visible over the Atlantic ocean except for an Atlantic Niño pattern at a lag of 0 months. A linear regression pattern was visible, however according to Cabos et al. (2019) inter annual variability in the TAV peaks in JJ in the central equatorial Atlantic (20°W-0°). Making the variability in SST high and therefore making a correlation unlikely. The Atlantic Niño pattern can be seen in Figure 33(c), where a negative difference in SST between the dry and wet composites suggests more evaporation over the origin area for warmer SST's and therefore more precipitation. The anomalous wind pattern in Figure 33(c) confirms the influence of the Atlantic Niño between wet and dry composites in the AMJJ season. The Bjerknes feedback generates westerly anomalies during the Atlantic Niño phase. Since the Atlantic Niño pattern is only visible without a lag, the skill for this season over the Atlantic is low. In Figure 22 it was seen that the AMJJ season has the largest sub-seasonal spread in precipitation of the three seasons. This, in combination with the vanishing of the skill of Atlantic Niño with increased lag time, gives reason to investigate sub seasonal forecast skill for the AMJJ season.

The ASON season shows only small correlation and regression patterns over the Atlantic. For a lag of 0 months a dipole is visible between the South and Nort Atlantic, with warmer temperatures in the south and colder temperatures in the north corresponding to more precipitation over Suriname. This would put the position of the ITCZ more towards the south and therefore more over Suriname. This was also seen in Figure 25(d). This is in agreement with a negative difference between the dry and wet composites SST. Again showing that higher SST causes more evaporation to occur and therefore more precipitation. Since these patters fade when adding lag time. The skill for precipitation forecasts in ASON does not lie in the Atlantic.

The processes relating precipitation in Suriname to the Atlantic SST and the position and intensity of the ITCZ are of shorter time duration, therefore the skill of seasonal forecast is not that high when seasonal precipitation anomalies depend on these processes. The skill lies in the processes that cause the SST change and the ITCZ shift, such as the AMM, generated by the WES-feedback and the Atlantic Niño generated by the Bjerknes feedback.

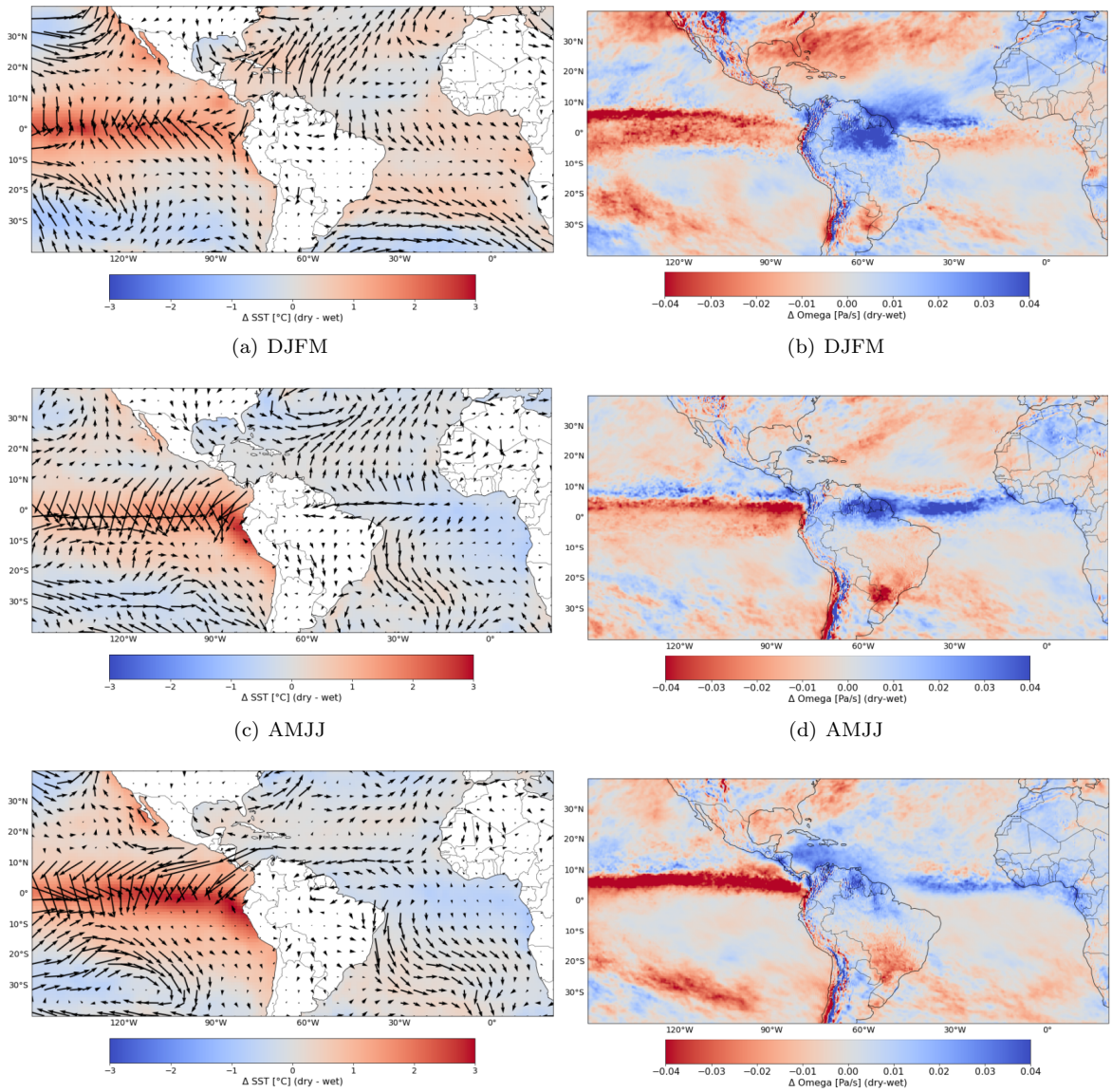


(a) DJFM (b) DJFM

(c) AMJJ (d) AMJJ

(e) ASON (f) ASON

**Figure 33:** On the left: Dry minus wet composites SST and 10m wind, and on the right: Dry minus wet vertical windspeed at 500m

## 6.2 Pacific sea surface temperature anomalies and El Nino Southern Oscillation

The Pacific SSTAs do not have a direct connection to the evaporation-precipitation path for Suriname. Nonetheless the correlations between the Pacific SSTA and Suriname precipitation anomalies are high. In the wet and dry season ENSO clearly has influence on the difference between the wet and dry composites. Both in surface windspeed and SST in Figure 33 it can be seen that in drier years ENSO causes warmer SST and strong convective winds. The same pattern can be found in the vertical wind speed difference between the wet and dry composites. In drier years there is more upward velocity in the Pacific around the equator and more downward velocity over the Atlantic and South America around the equator, which relates to El Nino conditions. ENSO is a pattern that can be predicted beforehand. The strong SST patterns that are needed to change the circulation patterns take time to evolve. Therefore the skill for seasonal forecasts for Suriname is stronger when the anomalies in seasonal precipitation are influenced by ENSO behaviour.

In the DJFM season the strongest correlation occurred along the Pacific equator without a lag. This same pattern can be viewed in Figure 33(a), where warm SST's in the Nino3.4 area [5S-5N,170W-120W] correspond to less precipitation over Suriname. In Figure 33(b) a difference in vertical wind speed is presented between the wet and the dry composites, this is in line with a change in the Walker circulation perturbed by El Niño conditions (see Appendix B).

The AMJJ correlation patterns over the Pacific relating to ENSO are not that pronounced. Still the same ENSO pattern as described for the DJFM season is visible in the composite map (Figure 33(c)). Though the vertical wind speed in Figure 33(d) shows a different pattern than for the DJFM season, suggesting less influences of a perturbation of the Walker circulation and more impact from a shift in the Hadley cell and therefore the ITCZ position.

The ASON correlations over the Pacific are strongest of the three seasons. Over the areas of Niño3 [5S-5N,150W-90W] and Niño3.4 [5S-5N,170W-120W] a clear negative correlation is visible. Suggesting drier conditions over Suriname during El Niño conditions. A clear ENSO pattern can also be established in the wet and dry composite difference between SST and wind patterns (Figure 33(e)). The strongest ASON corrrelation was found for 3 months of lagtime, therefore a composite of 3 month lag (MAMJ) for the ASON composite years was also viewed (Figure 34). Here the wind and SST anomalies over the Pacific indicating ENSO are even more pronounced. Easterly wind anomalies in the western equatorial Atlantic related to the Bjerknes feedback are visible. Due to the long lag time at which the ENSO correlations are visible for the ASON season there is a clear indication of skill for the prediction of precipitation anomalies.

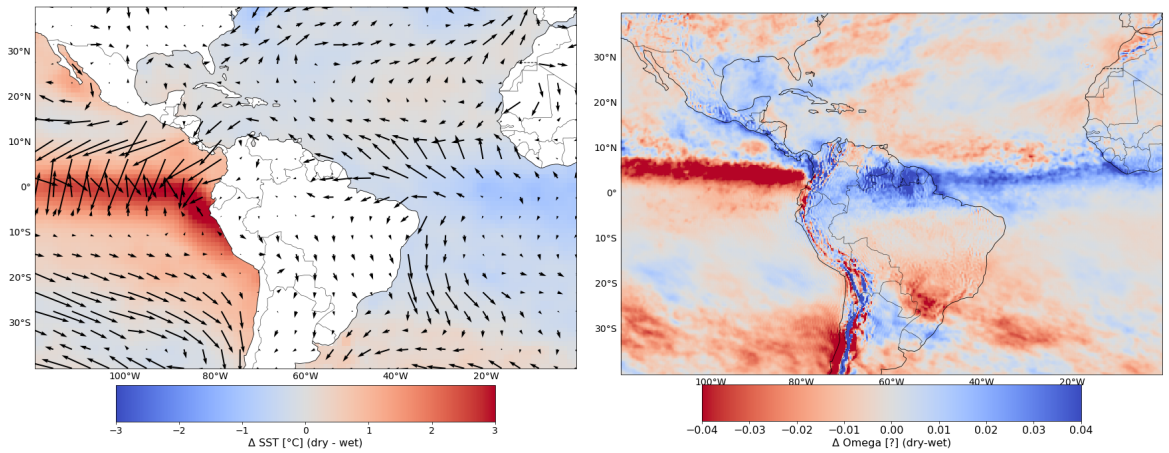


(a) ASON - Lag 3 months

(b) ASON - Lag 3 months

**Figure 34:** (a) Dry minus wet composites SST and 10m wind, (b) Dry minus wet vertical windspeed at 500m

In prior work by Nurmohamed et al. (2007) the correlation between precipitation over Suriname and ENSO indices was found to be a lot larger than the correlations that were found in this thesis report. No clear explanation could however be found why these differences occured. Nurmohamed et al. (2007) have looked at the relationship between precipitation variability in Suriname and the Atlantic SST anomalies and tropical Pacific ENSO SST anomalies. This was done on the basis of t-test and the Pearson correlation coefficient. High correlations were shown with the TSA SST (0.66 for SON with a 3-month lag, -0.52 for MAM with a 0-month lag), the Atlantic Nino SST (0.63 for SON with a 4-month lag, -0.52 for MAM with a 0-month lag) and the Nino1+2 SST (0.59 for MAM with a 1-month lag, -0.63 for DJF with a 3-month lag). The period JJA showed lower correlations to the observed SST patterns.

## 6.3 Teleconnections

The ENSO teleconnections have already been partly discussed in the previous sections, however the dynamics of ENSO are not the same for every El Niño or La Niña. Rodrigues et al. (2011) proposed that strong and long El Niño periods generate different SST variations over the Atlantic than weak and short El Niño periods. During strong and long El Niño, cold anomalies are generated in the Atlantic Cold Tongue (ACT) in boreal winter and spring, causing a positive AMM mode. Weak and short El Niño periods generate warm anomalies in the ACT in boreal winter and spring, causing a negative AMM mode. This could explain the relatively high SST and wind anomalies over the Pacific in Figure 33(a), in contrast to unexpected low correlation values in the DJFM season.

Since the recycling rate of moisture found with WAM2layers is very low in Suriname, the likelihood that the South American Monsoon System (SAMS) has an influence on the precipitation in Suriname is very low. Other than most South-American countries, Suriname is mainly influenced by ocean-atmosphere dynamics. However in the wet DJFM season the precipitation recycling ratio is higher and shows a significant difference between the wet and dry composite. This could indicate a potential influence of the SAMS. Especially considering the fact that the boreal winter is the time period of the rainy season of the SAMS. During boreal winter periods of strong (weak) SAMS convection occur over the Western Amazon. As a result strong (weak) subsidence over North Eastern Brazil occurs (Campos et al., 2022). This pattern of subsidence is visible in the vertical wind speed in Figure 33(b).

The influence of the Bjerkness in the AMJJ season in combination with a regression of over 1.5 [mm/d / °C] over the Pacific at 45°S, 90°W for a lag of 2 months, and regression seen on the east coast of Brazil, some influence of ENSO through the PSA is suggested.

Although the AMJJ season is the season with the largest spread in precipitation anomalies and therefore of high importance to seasonal predictions, it is the season with the lowest skill found for seasonal predictions. Bedward and Meerbeeck (2013) also found that AMJ was not well predicted by the CIMH 3-monthly tercile predictions. They suggested that including additional drivers of Caribbean seasonal rainfall into the predictions systems, such as the North Atlantic Oscillation (NAO), would cause improvement. The main predictor in the forecasting system of the CIMH is now ENSO. Mélice and Servain (2003) showed that the NAO leads the anomalies in the Tropical North Atlantic by 14 months, causing decadal variations in the Tropical Atlantic Meridional Gradient (TAMG).

## 6.4 Further study

In the analysis of GridPrecip the station gauge data is adopted as true. A deeper study on the accuracy and outliers of the station data would improve this analysis. Also composites that are used in this study are made up of a small number of years and for moisture tracking only the relevant wet and dry years are used. These are small sample sizes.

This thesis report is based upon monthly averaged values. Both for precipitation and predictors. It is very well possible that certain dynamics are not presented when looking only at the monthly averages. This includes also the onset of the seasons. For this study only the anomalies to the monthly values are studied, and therefore the intensity difference in precipitation per season. The change in the onset of the seasons was not incorporated in this study. For instance a study on the effects on the path of the ITCZ, instead of the intensity of the ITCZ, and therefore the onset of the seasons in Suriname would be of added value.

The drivers of anomalous precipitation in Suriname, as discussed in this study, are inherently interconnected and cannot be analyzed separate. The different drivers interact with one another. For instance, the inter-hemispheric temperature contrast of the Atlantic influences the positioning of the ITCZ. In turn, the ITCZ drives the dynamics of the tropical Atlantic ocean with changes in surface wind patterns. Further exploration into the impact of individual drivers on Suriname's precipitation anomalies, as opposed to the influence of multiple drivers reinforcing each other, would enhance the certainty of the areas of skill.

Lastly for relevant forecasts for stakeholders in Suriname it would be beneficial to expand this study towards daily or 5-days extremes of precipitation over Suriname. The Master's Thesis by Smit (2023) showed an increase in precipitation extremes in Suriname in the future in relation to climate change. 1% and 0.1% extremes are projected to increase at the end of the century for both 1-day and 5-day cumulative precipitation extremes. Preparing for these extremes is evident for many different stakeholders. Precipitation forecasts could potentially even be enhanced by including other parameters relevant to stakeholders, such as the occurrence of floods, river discharge and crop growth.

# 7 Conclusion

The research objective of this study is to look into the sources of the predictive skill for seasonal precipitation forecasts for Suriname. This was done by performing moisture tracking with WAM2layers, producing maps of sea surface temperature anomalies (SSTA) correlations, maps of the slope of linear regressions and looking at composite data, such as vertical wind speed, SST and wind at 850hPa of wet and dry precipitation composites. .

The gridded precipitation sets used in this study showed good correlation, RMSE and bias values compared to station data and can therefore be used when a long time series of precipitation for Suriname is required. Care should be taken when shifting from monthly precipitation values to daily precipitation values. ERA5 shows the lowest compatibility with the station observations.

The precipitation anomalies of the DJFM season for Suriname are mainly determined by SST behaviour over the Atlantic. Pacific SST has less influence on the DJFM season. When looking at the DJFM season composites, evidence is found of a link between precipitation anomalies and the Atlantic Meridional Mode. The tropical Atlantic variability has an influence on the position of the ITCZ and precipitation anomalies over Suriname, which is a process that does show skill 1-2 months prior for Suriname. Most skill however would be found in processes excarbating the TAV, such as the WES-feedback and the NAO. The influence of ENSO on the precipitation anomalies over Suriname in the DJFM season consist mainly of the change in Walker circulation.

The AMJJ season is the season with the least amount of predictive skill for the anomalies of precipitation over Suriname. Both Atlantic and Pacific SST influences the precipitation anomalies, however only without a lag between SSTA and precipitation anomalies. When a lag is introduced the skill vanishes. Therefore with the climatic processes studied in this report no clear predictive skill can be found for the AMJJ season. Some further investigation could be done into the sub-seasonal precipitation and processes in the AMJJ season.

The ASON season precipitation over Suriname is dominated by the influence of ENSO patterns. Since the ENSO patterns are most pronounced during the earlier months of the year, the predictive skill for ASON precipitation anomalies based upon ENSO conditions is present. ASON suggests the largest amount of skill to predict seasonal precipitation anomalies, compared to the AMJJ and DJFM seasons.

The processes of potential skill found in this thesis report can be of help to forecasters for the improvement of seasonal precipitation forecasts for Suriname. The addition of moisture tracking with WAM2layers to sea surface temperature correlations does give more insight into why certain correlations occur. It helps to find the teleconnection patterns connected to the precipitation anomalies. Nevertheless, most of the information on the skill for seasonal precipitation anomalies in this thesis comes from SST correlations and composite data.

# References


Adler, R. F., Huffman, G. J., Chang, A., Ferraro, R., Xie, P.-P., Janowiak, J., Rudolf, B., Schneider, U., Curtis, S., Bolvin, D., Gruber, A., Susskind, J., Arkin, P., & Nelkin, E. (2003). *The Version-2 Global Precipitation Climatology Project (GPCP) Monthly Precipitation Analysis (1979-Present)* (tech. rep.). http://precip.gsfc.nasa.gov

Ahmed, K., Shahid, S., Wang, X., Nawaz, N., & Najeebullah, K. (2019). Evaluation of gridded precipitation datasets over arid regions of Pakistan. *Water (Switzerland)*, *11*(2). https://doi.org/10.3390/w11020210

Alexander, M. A., Newman, M., Lanzante And, J. R., Lau, N.-C., & Scott, J. D. (n.d.). *The Atmospheric Bridge: The Influence of ENSO Teleconnections on Air-Sea Interaction over the Global Oceans* (tech. rep.).

Amaya, D. J., DeFlorio, M. J., Miller, A. J., & Xie, S.-P. (2017). WES feedback and the Atlantic Meridional Mode: observations and CMIP5 comparisons. *Climate Dynamics*, *49*(5-6), 1665–1679. https://doi.org/10.1007/s00382-016-3411-1

Antich-Homar, H., Hess, K., Solaun, K., Alleng, G., & Flores, A. (2022). An Integrated Approach for Evaluating Climate Change Risks: A Case Study in Suriname. *Sustainability (Switzerland)*, *14*(3). https://doi.org/10.3390/su14031463

Ayoub, A. B., Tangang, F., Juneng, L., Tan, M. L., & Chung, J. X. (2020). Evaluation of gridded precipitation datasets in Malaysia. *Remote Sensing*, *12*(4). https://doi.org/10.3390/rs12040613

Bedward, S., & Meerbeeck, C. J. (2013). *Assessing the skill of seasonal rainfall outlooks for the Caribbean Variability of the Panama Low and its impact on Caribbean early season rainfall View project CCASAP View project* (tech. rep.). https://www.researchgate.net/publication/258776249

Byrne, M. P., Pendergrass, A. G., Rapp, A. D., & Wodzicki, K. R. (2018). Response of the Intertropical Convergence Zone to Climate Change: Location, Width, and Strength. https://doi.org/10.1007/s40641-018-0110-5

Cabos, W., de la Vara, A., & Koseki, S. (2019). Tropical Atlantic Variability: Observations and modeling. https://doi.org/10.3390/atmos10090502

Campos, M. C., Chiessi, C. M., Novello, V. F., Crivellari, S., Campos, J. L. P. S., Albuquerque, A. L. S., Venancio, I. M., Santos, T. P., Melo, D. B., Cruz, F. W., Sawakuchi, A. O., & Mendes, V. R. (2022). South American precipitation dipole forced by interhemispheric temperature gradient. *Scientific Reports*, *12*(1), 10527. https://doi.org/10.1038/s41598-022-14495-1

Córdova, M., Célleri, R., & van Delden, A. (2022). Dynamics of Precipitation Anomalies in Tropical South America. *Atmosphere*, *13*(6). https://doi.org/10.3390/atmos13060972

Dittus, A. J., Karoly, D. J., Donat, M. G., Lewis, S. C., & Alexander, L. V. (2018). Understanding the role of sea surface temperature-forcing for variability in global temperature and precipitation extremes. *Weather and Climate Extremes*, *21*, 1–9. https://doi.org/10.1016/j.wace.2018.06.002

Donohoe, A., Marshall, J., Ferreira, D., & Mcgee, D. (2013). The relationship between ITCZ location and cross-equatorial atmospheric heat transport: From the seasonal cycle to the last glacial maximum. *Journal of Climate*, *26*(11), 3597–3618. https://doi.org/10.1175/JCLI-D-12-00467.1

Ferreira, G. W., & Reboita, M. S. (2022). A New Look into the South America Precipitation Regimes: Observation and Forecast. *Atmosphere*, *13*(6). https://doi.org/10.3390/atmos13060873

Ferreira, G. W., Reboita, M. S., & Drumond, A. (2022). Evaluation of ECMWF-SEAS5 Seasonal Temperature and Precipitation Predictions over South America. *Climate*, *10*(9). https://doi.org/10.3390/cli10090128

Fortuin, J. P., Becker, C. R., Fujiwara, M., Immler, F., Kelder, H. M., Scheele, M. P., Schrems, O., & Verver, G. H. (2007). Origin and transport of tropical cirrus clouds observed over Paramaribo, Suriname (5.8°N, 55.2°W). *Journal of Geophysical Research Atmospheres*, *112*(9). https://doi.org/10.1029/2005JD006420

Funk, C., Peterson, P., Landsfeld, M., Pedreros, D., Verdin, J., Shukla, S., Husak, G., Rowland, J., Harrison, L., Hoell, A., & Michaelsen, J. (2015). The climate hazards infrared precipitation with stations—a new environmental record for monitoring extremes. *Scientific Data*, *2*(1), 150066. https://doi.org/10.1038/sdata.2015.66

Gao, F., Chen, X., Yang, W., Wang, W., Shi, L., Zhang, X., Liu, Y., & Tian, Y. (2022). Statistical characteristics, trends, and variability of rainfall in Shanxi province, China, during the period

1957–2019. *Theoretical and Applied Climatology*, *148*(3-4), 955–966. https://doi.org/10.1007/s00704-022-03924-w

Gersie, K. S., Van Balen, R. T., & Kroonenberg, S. B. (2021). The Interplay between Tectonic Activity, Climate and Sea-Level Change in the Suriname River Valley, Tropical South America. *Quaternary*, *4*(2), 11. https://doi.org/10.3390/quat4020011

Harris, I., Osborn, T. J., Jones, P., & Lister, D. (2020). Version 4 of the CRU TS monthly high-resolution gridded multivariate climate dataset. *Scientific Data*, *7*(1). https://doi.org/10.1038/s41597-020-0453-3

Hersbach, H., Bell, B., Berrisford, P., Hirahara, S., Horányi, A., Muñoz-Sabater, J., Nicolas, J., Peubey, C., Radu, R., Schepers, D., Simmons, A., Soci, C., Abdalla, S., Abellan, X., Balsamo, G., Bechtold, P., Biavati, G., Bidlot, J., Bonavita, M., ... Thépaut, J.-N. (2020). The ERA5 global reanalysis. *Quarterly Journal of the Royal Meteorological Society*, *146*(730), 1999–2049. https://doi.org/10.1002/qj.3803

Koudahe, K., Kayode, A. J., Samson, A. O., Adebola, A. A., & Djaman, K. (2017). Trend Analysis in Standardized Precipitation Index and Standardized Anomaly Index in the Context of Climate Change in Southern Togo. *Atmospheric and Climate Sciences*, *07*(04), 401–423. https://doi.org/10.4236/acs.2017.74030

Kumar, A., Ceron, J.-P., Coelho, C., Ferranti, L., Graham, R., Jones, D., Merryfield, W., Muñoz, Á., Pai, S., & Rodriguez, E. (2020). *Guidance on Operational Practices for Objective Seasonal Forecasting* (tech. rep.). World Meteorological Organization (WMO).

Lorenz, E. N. (1982). Atmospheric predictability experiments with a large numerical model. *Tellus*, *34*(6), 505–513.

Marengo, J. A., Liebmann, B., Grimm, A. M., Misra, V., Silva Dias, P. L., Cavalcanti, I. F., Carvalho, L. M., Berbery, E. H., Ambrizzi, T., Vera, C. S., Saulo, A. C., Nogues-Paegle, J., Zipser, E., Seth, A., & Alves, L. M. (2012). Recent developments on the South American monsoon system. https://doi.org/10.1002/joc.2254

Marshall, J., Donohoe, A., Ferreira, D., & McGee, D. (2014). The ocean's role in setting the mean position of the Inter-Tropical Convergence Zone. *Climate Dynamics*, *42*(7-8), 1967–1979. https://doi.org/10.1007/s00382-013-1767-z

Martinez, C., Goddard, L., Kushnir, Y., & Ting, M. (2019). Seasonal climatology and dynamical mechanisms of rainfall in the Caribbean. *Climate Dynamics*, *53*(1-2), 825–846. https://doi.org/10.1007/s00382-019-04616-4

Meerbeeck, C. V. (2013). *CARICOF-The Caribbean Regional Climate Outlook Forum* (tech. rep.).

Mélice, J.-L., & Servain, J. (2003). The tropical Atlantic meridional SST gradient index and its relationships with the SOI, NAO and Southern Ocean. *Climate Dynamics*, *20*(5), 447–464. https://doi.org/10.1007/s00382-002-0289-x

Naipal, S., & Nurmohamed, R. (2004). *Trends And Variation In Monthly Rainfall And Temperature In Suriname* (tech. rep.). http://conservewater.melbournewater.com.au/content/conserve/el_nino_years.htm,

Nogueira, M. (2020). Inter-comparison of ERA-5, ERA-interim and GPCP rainfall over the last 40 years: Process-based analysis of systematic and random differences. *Journal of Hydrology*, *583*. https://doi.org/10.1016/j.jhydrol.2020.124632

Nurmohamed, R., Naipal, S., & Becker, C. (2007). Rainfall variability in Suriname and its relationship with the tropical Pacific ENSO SST anomalies and the Atlantic SST anomalies. *International Journal of Climatology*, *27*(2), 249–256. https://doi.org/10.1002/joc.1374

Peel, M. C., Finlayson, B. L., & Mcmahon, T. A. (2007). *Updated world map of the Köppen-Geiger climate classification* (tech. rep.). www.hydrol-earth-syst-sci.net/11/1633/2007/

Rayner, N. A., Parker, D. E., Horton, E. B., Folland, C. K., Alexander, L. V., Rowell, D. P., Kent, E. C., & Kaplan, A. (2003). Global analyses of sea surface temperature, sea ice, and night marine air temperature since the late nineteenth century. *Journal of Geophysical Research: Atmospheres*, *108*(14). https://doi.org/10.1029/2002jd002670

Reboita, M. S., Ambrizzi, T., Crespo, N. M., Dutra, L. M. M., Ferreira, G. W. d. S., Rehbein, A., Drumond, A., da Rocha, R. P., & Souza, C. A. d. (2021). Impacts of teleconnection patterns on South America climate. *Annals of the New York Academy of Sciences*, *1504*(1), 116–153. https://doi.org/10.1111/nyas.14592

Ríos-Cornejo, D., Penas, Á., Álvarez-Esteban, R., & del Río, S. (2015). Links between teleconnection patterns and precipitation in Spain. *Atmospheric Research*, *156*, 14–28. https://doi.org/10.1016/j.atmosres.2014.12.012

Rodrigues, R. R., Haarsma, R. J., Campos, E. J. D., & Ambrizzi, T. (2011). The Impacts of Inter–El Niño Variability on the Tropical Atlantic and Northeast Brazil Climate. *Journal of Climate*, *24*(13), 3402–3422. https://doi.org/10.1175/2011JCLI3983.1

Satgé, F., Defrance, D., Sultan, B., Bonnet, M. P., Seyler, F., Rouché, N., Pierron, F., & Paturel, J. E. (2020). Evaluation of 23 gridded precipitation datasets across West Africa. *Journal of Hydrology*, *581*. https://doi.org/10.1016/j.jhydrol.2019.124412

Schneider, T., Bischoff, T., & Haug, G. H. (2014). Migrations and dynamics of the intertropical convergence zone. https://doi.org/10.1038/nature13636

Schneider, U., Hänsel, S., Finger, P., Rustemeier, E., & Ziese, M. (2022). GPCC Full Data Monthly Product Version 2022 at 0.25°: Monthly Land-Surface Precipitation from Rain-Gauges built on GTS-based and Historical Data.

Schumacher, V., Justino, F., Fernández, A., Meseguer-Ruiz, O., Sarricolea, P., Comin, A., Peroni Venancio, L., & Althoff, D. (2020). Comparison between observations and gridded data sets over complex terrain in the Chilean Andes: Precipitation and temperature. *International Journal of Climatology*, *40*(12), 5266–5288. https://doi.org/10.1002/joc.6518

Smit, J. (2023). Impact of climate change on precipitation in Suriname.

Solaun, K., Alleng, G., Flores, A., Resomardono, C., Hess, K., & Antich, H. (2021). *State of the Climate Report: Suriname Climate Change Division* (tech. rep.). http://www.iadb.org

Taschetto, A. S., & Wainer, I. (2008). Reproducibility of South American precipitation due to subtropical South Atlantic SSTs. *Journal of Climate*, *21*(12), 2835–2851. https://doi.org/10.1175/2007JCLI1865.1

Van Der Ent, R. J., Savenije, H. H. G., Schaefli, B., & Steele-Dunne, S. C. (2010). Origin and fate of atmospheric moisture over continents. *Water Resources Research*, *46*(9). https://doi.org/10.1029/2010WR009127

Van Der Ent, R. J., Benedict, I. B., Weijenborg, C., Cömert, T., van de Koppel, N., Guo, L., & Kalverla, P. (2022). WAM2layers. https://doi.org/10.5281/zenodo.7010594

Van Der Ent, R. J., Wang-Erlandsson, L., Keys, P. W., & Savenije, H. H. G. (2014). Contrasting roles of interception and transpiration in the hydrological cycle – Part 2: Moisture recycling. *Earth System Dynamics*, *5*(2), 471–489. https://doi.org/10.5194/esd-5-471-2014

van Oldenborgh, G. J., Hendon, H., Stockdale, T., L'Heureux, M., Coughlan de Perez, E., Singh, R., & van Aalst, M. (2021). Defining El Niño indices in a warming climate. *Environmental Research Letters*, *16*(4), 044003. https://doi.org/10.1088/1748-9326/abe9ed

World Meteorological Organization. (2011). *Guide to Climatological Practices* (tech. rep.). World Meteorological Organization. Geneva, Switzerland.

Ziese, M., Rauthe-Schöch, A., Becker, A., Finger, P., Rustemeier, E., Hänsel, S., & Schneider, U. (2022). GPCC Full Data Daily Version 2022 at 1.0°: Daily Land-Surface Precipitation from Rain-Gauges built on GTS-based and Historic Data.

# A Quality Control LACA&D

The quality control of the LACA&D observational data set is done in a similar way as for the ECA&D data set. This entails:

**Data import**

The data comes in various file formats. Importing this data into the database tables is entirely done by hand, running relevant scripts to do the conversions. The conversions differ for each data source.

The data is stored in the form of daily precipitation values. Whenever synoptical 12-hourly precipitation data is available at 06 and 18 UT, daily precipitation is calculated as the sum the precipitation of 18UT of the current day and precipitation of 6 UT of the next day.

**Quality control**

During the quality control each individual observation in a series is flagged as one of the following three flags:

- Flag=0: observation is valid
- Flag=1: observation is suspect
- Flag=9: observation is missing

If a daily precipitation amount does not adhere to the following conditions it is flagged as suspect:

- observation must be equal to or exceed 0 mm
- observation must be less than 300.0 mm
- observation must not be repetitive (i.e. exactly the same amount) for 10 days in a row if the amount is larger than 1.0 mm
- observation must not be repetitive (i.e. exactly the same amount) for 5 days in a row if the amount is larger than 5.0 mm
- dry periods receive a flag = 1 (suspect), if the amount of dry days lies outside a 14·bivariate standard deviation

The criteria are assessed through an automated process, but a manual intervention is possible for non-blended series and the manual quality control flag will be propagated to the blended series. For instance, precipitation extremes that are flagged 'suspect' are overruled if additional evidence exists (e.g. from radar images or weather charts) that the particular extreme is plausible.

# B Walker Circulation ENSO

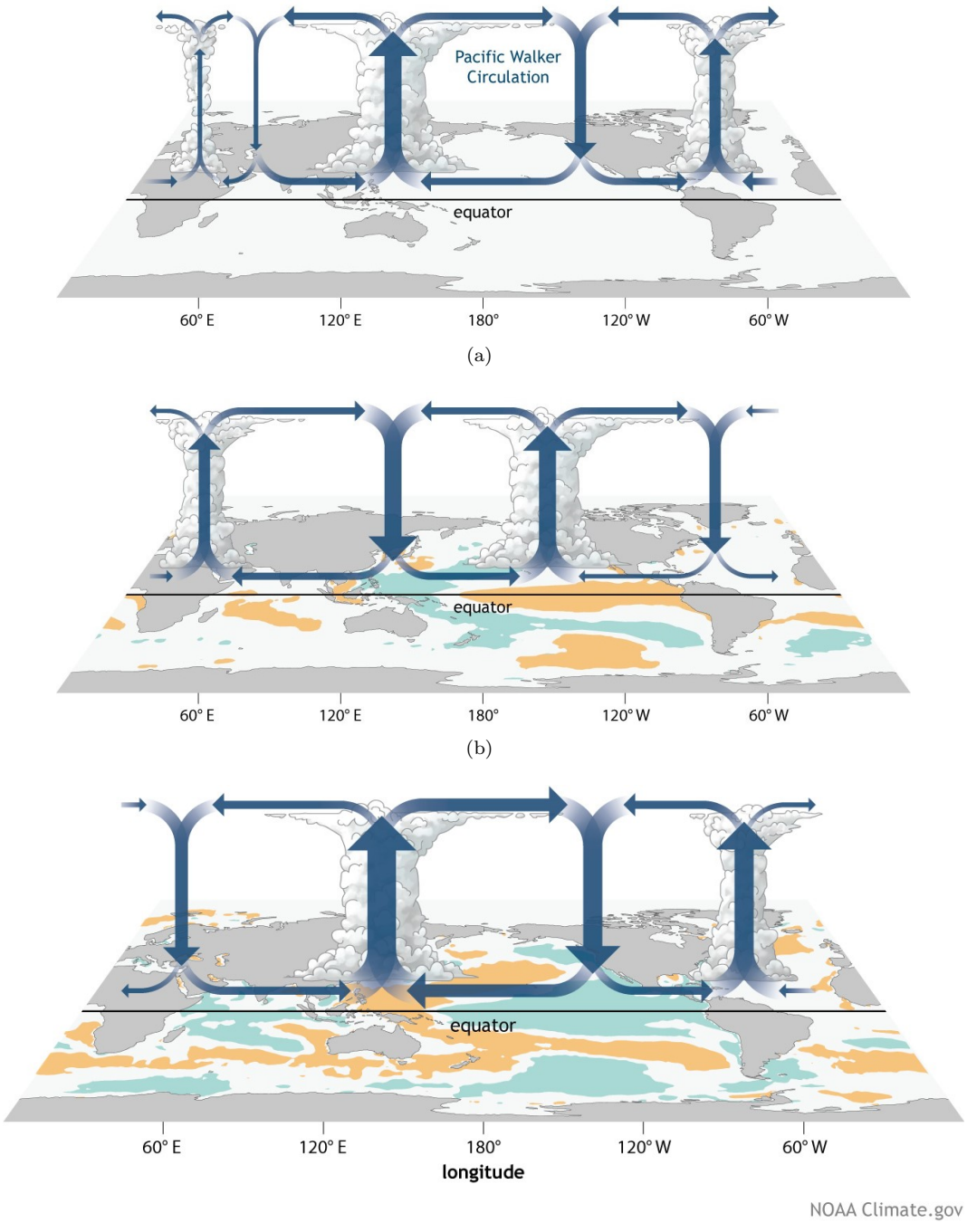


**Figure 35:** Generalized Walker Circulation (December-February) during (a) ENSO-neutral conditions (b) El Niño events (c) La Niña events. (Illustration by NOAA Climate.gov drawing by Fiona Martin)

# C Correlation with indices

**Table 17:** Spearman correlation between predefined indices and precipitation anomalies. Correlations that are significant with p $\leq$ 0.05 (p $\leq$ 0.01) are indicated with an * (**).

| Index | Correlation (DJF) | Correlation (MAM) | Correlation (JJA) | Correlation (SON) |
|---|---|---|---|---|
| Nino12 | $r_{lag3} = 0.036$ | $r_{lag1} = 0.016$ | $r_{lag0} = -0.47^{**}$ | $r_{lag0} = -0.38^{**}$ |
| Atl Nino | $r_{lag0} = -0.20^{**}$ | $r_{lag0} = -0.24^{**}$ | - | $r_{lag4} = -0.020$ |
| TNA | $r_{lag11-12} =$ | $r_{lag0} = -0.24$ | - | - |
| TSA | $r_{lag3} = -0.035$ | $r_{lag0} = -0.26^{**}$ | $r_{lag0} = 0.28^{**}$ | $r_{lag3} = -0.013$ |

**Table 18:** Correlation Nurmohamed et al. (2007).

| Index | Correlation (DJF) | Correlation (MAM) | Correlation (JJA) | Correlation (SON) |
|---|---|---|---|---|
| Nino12 | $r_{lag3} = -0.63$ | $r_{lag1} = 0.59$ | $r_{lag0-1} = -0.52$ | $r_{lag0} = -0.57$ |
| Atl Nino | $r_{lag0} = -0.36$ | $r_{lag0} = -0.52$ | - | $r_{lag4} = 0.63$ |
| TNA | $r_{lag11-12} = 0.23$ | $r_{lag0} = 0.23$ | - | - |
| TSA | $r_{lag3} = -0.24$ | $r_{lag0} = -0.52$ | $r_{lag0} = -0.52$ | $r_{lag3} = 0.66$ |

# D Spatial pattern precipitation with winds at 200hPa and 10m

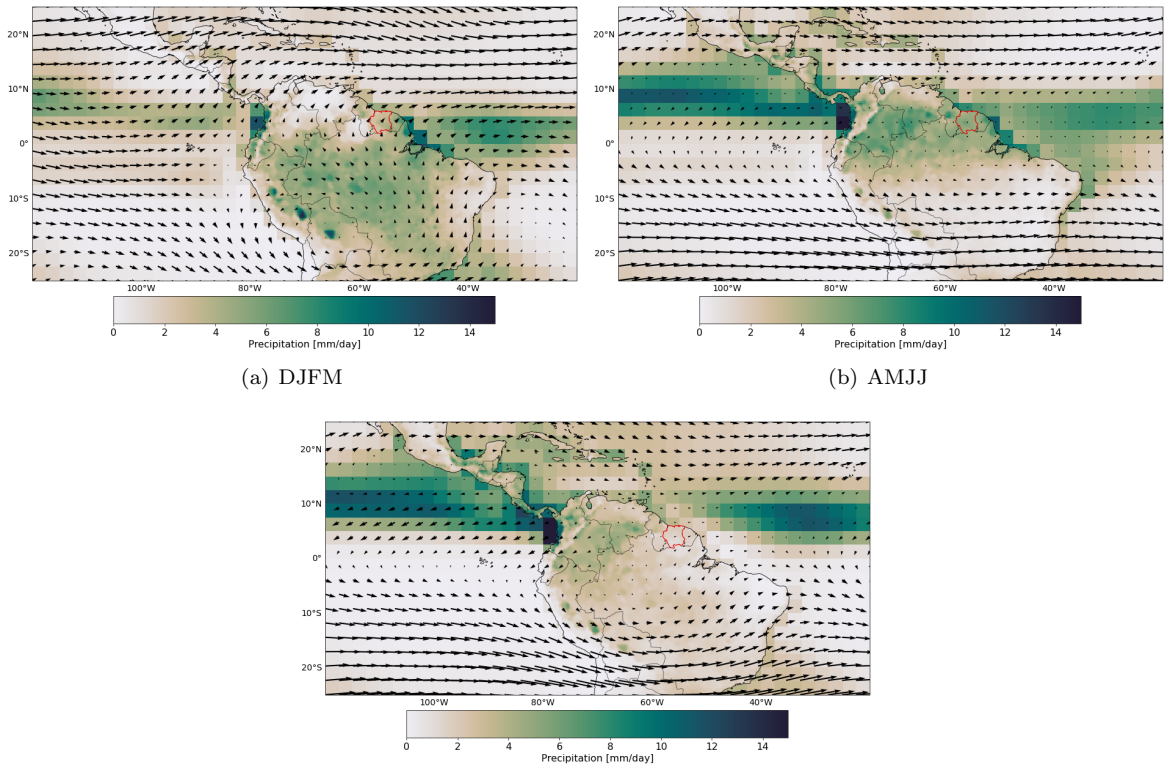


(a) DJFM

(b) AMJJ

(c) ASON

**Figure 36:** Spatial pattern of precipitation (GPCP over ocean and GPCC over land) and 200hPa wind (ERA5) for the period 1981-2020

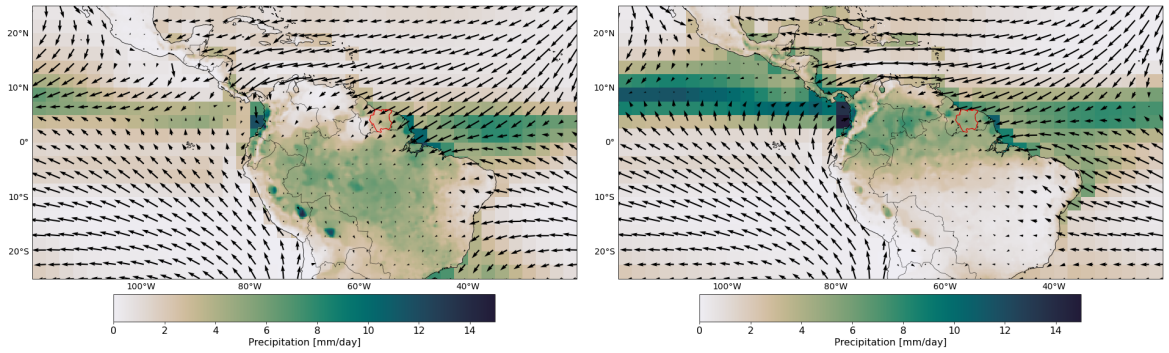


(a) DJFM




(b) AMJJ

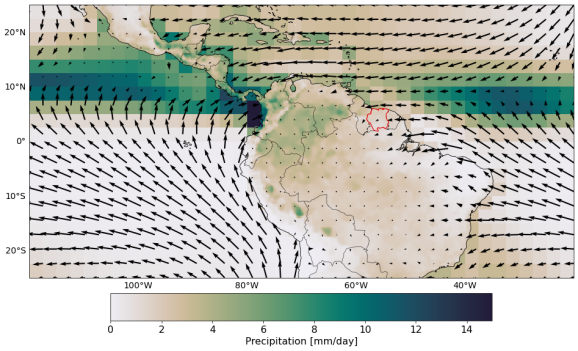


(c) ASON

**Figure 37:** Spatial pattern of precipitation (GPCP over ocean and GPCC over land) and 10m wind (ERA5) for the period 1981-2020

# E Station gauge density maps GPCC

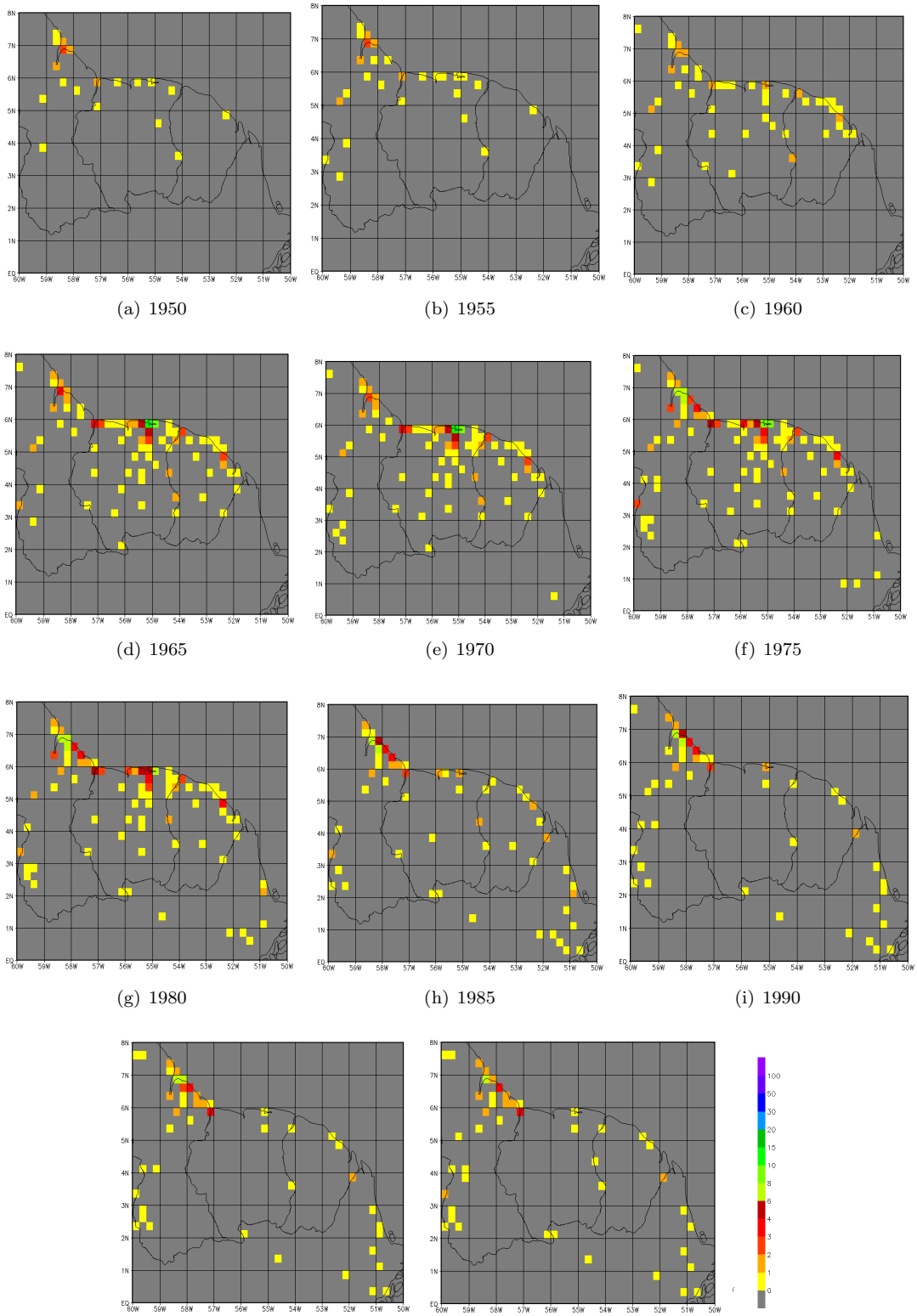


(a) 1950 (b) 1955 (c) 1960

(d) 1965 (e) 1970 (f) 1975

(g) 1980 (h) 1985 (i) 1990

(j) 1995 (k) 2000 (l)

**Figure 38:** Station density maps per gridcell for GPCC data